

See discussions, stats, and author profiles for this publication at: <https://www.researchgate.net/publication/227193931>

Quantitative Colocalisation Imaging: Concepts, Measurements, and Pitfalls

CHAPTER · DECEMBER 2006

DOI: 10.1007/978-3-540-71331-9_5

CITATIONS

12

READS

76

2 AUTHORS:



[Martin Oheim](#)

French National Centre for Scientific Resea...

63 PUBLICATIONS 2,119 CITATIONS

[SEE PROFILE](#)



[Dongdong Li](#)

INSERM (National Institute of Health and M...

21 PUBLICATIONS 350 CITATIONS

[SEE PROFILE](#)

5

Quantitative Colocalisation Imaging: Concepts, Measurements, and Pitfalls

Martin Oheim and Dongdong Li

Abstract Many questions in cell biology and biophysics involve the quantitation of the colocalisation of proteins tagged with different fluorophores and their interaction. However, the incomplete separation of the different colour channels due to the presence of autofluorescence, along with cross-excitation and emission ‘bleed-through’ of one colour channel into the other, all combine to render the interpretation of multi-band images ambiguous. Traditionally often used in a qualitative manner by simply overlaying fluorescence images ('red plus green equals yellow'), multicolour fluorescence is increasingly moving away from static dual-colour images towards more quantitative studies involving the investigation of dynamical three-dimensional interaction of proteins tagged with different fluorophores in live cells. Quantifying fluorescence resonance energy transfer efficiency, fluorescence complementation and colour merging following photoactivation or photoswitching provide related examples in which quantitative image analysis of multicolour fluorescence is required. Despite its widespread use, reliable standards for evaluating the degree of spectral overlap in multicolour fluorescence and calculating quantitative colocalisation estimates are missing. In this chapter, using a number of intuitive yet practical examples, we discuss the factors that affect image quality and study their impact on the measured degree of colocalisation. We equally compare different pixel-based and object-based descriptors for analysing colocalisation of spectrally separate fluorescence. Finally, we discuss the use of spectral imaging and linear unmixing to study the presence in a ‘mixed pixel’ of spectrally overlapping fluorophores and discuss how this technique can be used to provide quantitative colocalisation information in more complex experimental scenarios in which classic dual- or triple-colour fluorescence would produce erroneous results.

5.1 Introduction

During the past 15 years there has been a remarkable growth in the use of fluorescence imaging in biological microscopy. This development has been largely driven by the generation and widespread use of fluorescent protein chimeras (reviewed in

Shaner et al. 2005; Giepmans 2006). Also, three-dimensional imaging at the subcellular level has become possible for many researchers with the broad availability of confocal and two-photon-excited fluorescence (2PEF) microscopes to many laboratories and imaging platforms. After the identification of the key molecules and signalling pathways, many questions in cell biology and cell biophysics concern where and when these molecules interact (Schultz et al. 2005). As a consequence, microscopic multicolour imaging is moving away from classical confocal immunofluorescence (Miyashita 2004) towards studies that typically involve the quantification of the dynamics of the three-dimensional expression and –ideally– interaction of proteins tagged with different fluorophores in live cells. Information on molecular interaction could be derived by adding information derived from fluorescence resonance energy transfer (FRET) (Jares-Erijman and Jovin 2003), fluorescence complementation assays (Kerrpola 2006), or colour merging following photoactivation or photoswitching (Betzig et al. 2006; Chudakov et al. 2006; Hess et al. 2006). Thus, larger and highly dimensional data sets must be handled.

Colocalisation studies using fluorescence imaging represent a powerful method for exploring putative associations between molecules and their targeting to discrete intracellular compartments. Ideally, several spectrally well-distinct fluorophores would be specifically addressed to their molecular-scale targets and imaged into distinct, spectrally separated detection channels so that the fluorescence intensity in each channel would contain spatial and concentration information exclusively derived from one fluorophore. These images could then be pseudocolour-coded displayed side by side or overlaid and the amount of colocalisation could be estimated from these intensity maps. Red and green equals yellow. The estimation of protein expression and colocalisation can be broken down to two steps: first, the selective labelling with and imaging of different fluorophores, followed by the quantification of their colocalisation from multicolour images. Both of these steps are based on hypotheses, for example that all collected fluorescence originates from endogenous label, and rely on the correct expression and subcellular targeting of fusion proteins, the existence of only negligible cross-talk between acquisition channels, or the linearity and spatial homogeneity of the analysed images.

In a real experiment, however, every one of the underlying assumptions is probably violated to some extent. Two simple questions arise:

1. To what extent are the spatial, spectral, and (to a lesser degree) temporal images truly independent?
2. How can we quantify the degree of colocalisation from such fluorescence images?

The aim of this chapter is to discuss the problems associated with the different techniques for dual-colour imaging and quantifying colocalisation and to evaluate their respective performance and limitations. Considering the microscope as a linear imaging device, we can describe the image of an arbitrary object as the linear superposition of point images of different intensity. We therefore restrict our discussion to imaging (subresolution) point objects. The generalisation to extended objects is straightforward.

The chapter is organised as follows: we first (Sect. 5.1.1) introduce a synthetic yet realistic dual-colour example that we will use throughout this chapter to study the

impact of different image parameters on the colocalisation estimate and to evaluate different strategies to quantify colocalisation. This example has the virtue that we can know and control the true amount of colocalisation between probes and can vary their degree of spectral overlap and relative brightness, vary the image noise and background offset in a controlled manner, and study their impact on the colocalisation estimate. In Sect. 5.1.2, we stress the importance of matching dyes, filters, and intermediate optical components by regarding (Box 5.1) step by step the process of choosing appropriate combinations in a realistic experiment. Box 5.2 offers a swift review of optical sectioning techniques that can improve the colocalisation detection.

Box 5.1 Tracing spectral throughput along the excitation and emission optical path

The goal of dual-colour fluorescence microscopy is to simultaneously map the location and dynamics of two fluorescent vesicle markers from a dual-colour image pair. Multicolour maps are only as good as the raw images that are used to calculate them.

We here develop a simple rationale to chose optimal filters for a given fluorophore pair and to estimate the cross-talk that is engendered by filter mismatch. A more complete treatment can be found as an online resource on the Oheim laboratory Web site (Oheim et al. 2007). In the simplest case of only two fluorophores and negligible (or spatially and spectrally uniform) background, the fluorophore separation only depends on their excitation and emission spectral overlap and the filter bands used to isolate them. Neglecting higher-order effects (fluorophore saturation, self-absorption, aggregate formation and quenching, bleaching), the measured intensity (in analogue/digital [A/D] units) of a fluorophore on a microscopic image depends linearly on

1. The fluorophore spectral *extinction* $\epsilon(\lambda)$, which describes the probability of absorbing a photon at wavelength λ and is typically given as $\epsilon \times F_{\text{abs}}(\lambda)$, where ϵ is the *molar extinction coefficient* (mostly but not always specified at peak absorption) and $F_{\text{abs}}(\lambda)$ is the fluorophore absorption spectrum, with the peak absorption normalised to 1. ϵ is of the order of $61,000 \text{ mol}^{-1} \text{ cm}^{-1}$ for pEGFP-N1 (Clontech) and $48,000 \text{ mol}^{-1} \text{ cm}^{-1}$ for FM4-64 (Invitrogen). The curves for $F_{\text{abs}}(\lambda)$ are given in Fig. 5.6b. We next trace along the microscope light path (Fig. 5.6a, inset), starting from the light source¹, the fraction of the excitation light (black line) that is transmitted by the intermediate optical components and reaches the sample to excite the fluorophores.

(continued)

¹ The black line is the normalised experimental spectral distribution of the excitation light source used – here, a TILL polychrome II with about 20-nm excitation bandwidth. Alternatively, one could substitute here the transmission spectrum of an emission bandpass filter multiplied with the spectral emission of the Xe or Hg arc lamp.

Box 5.1 (continued)

Next, the dashed blue line shows the *reflectance* (1 minus transmission, neglecting absorption) of the primary dichroic beamsplitter.

2. The *fluorescence quantum yield* ϕ of a fluorophore defines the probability of an excited molecule relaxing to the ground state by emitting a fluorescence photon. The probability of emitting a photon at wavelength λ is obtained by multiplying ϕ with the normalised ($\int F_{\text{em}}(\lambda)d\lambda = 1$) fluorescence emission spectrum $F_{\text{em}}(\lambda)$. $\phi=0.60$ for enhanced-green fluorescent protein (EGFP; Patterson et al. 1997). In the absence of specific information for FM4-64 in lipid membranes (Bill Betz, Denise Lo Invitrogen, personal communications), we equally assumed 0.6 for FM4-64 (Table 5.1). The product $\epsilon\phi$ is sometimes referred to as the *fluorophore brightness*. The most absorptive fluorophores absorb more than 2 orders of magnitude more efficiently than the least. This is in stark contrast to the quantum efficiency, which typically falls in the range from 0.25 to 0.9 for most useful fluorophores, so they will not differ by more than a factor of 3–4 at most. As a result, ϕ will be of secondary importance in determining brightness.

Table 5.1 Spectroscopic properties of enhanced-green fluorescent protein (EGFP) and FM4-64

λ_{ex} , peak (nm)	ϵ (mol $^{-1}$ cm) $^{-1}$	λ_{em} , peak (nm)	ϕ	Comment
EGFP 50 mM HEPES, pH 7.5	488	61,000 ^a	509	0.6 ^b
FM4-64 Measured in CHCl ₃	558	48,000	734	0.6 ^c

HEPES N-(2-hydroxyethyl)piperazine-N'-ethanesulfonic acid

^aCubitt et al. (1999)

^bPatterson et al. (1997)

^cFM dyes are almost non-fluorescent in water, but their quantum yield increases about 350 times when they partition into a hydrophobic environment. (Henkel et al. 1996). The actual ϕ value in a lipid is hard to determine, as the concentration is typically not known. We therefore simply assumed that FM4-64 and EGFP have the same quantum efficiency.

3. The fluorophore *concentration* c , in moles per litre, or its density, e.g. for membrane-resident dyes.
4. The camera exposure or, more generally, detector *integration time*.
5. The fluorescence excitation volume (related to the objective optical depth, along the z -axis and illuminated area (xy), and thus to the numerical aperture (NA); however, not in two-photon-excited fluorescence).
6. The fraction of fluorescence collected (i.e. the solid angle covered by the NA).
7. The fluorescence collection volume (in the case of confocal apertures or directional-emission detection; Axelrod 2001).
8. The A/D unit, i.e. the number of counts per detected electron/pixel.

9. Light flux (illumination intensity) and detector response (detector quantum yield).

We consider here a single-excitation side-by-side projection of two colour-channel images (Fig. 5.6a, inset); we only compare the relative contribution of isomolar EGFP and FM4-64 to each colour-channel image, *ceterum paribus*. Given the narrow spectral width of the excitation, we neglected the spectral profile of the light source, which is set unity for all λ . To estimate cross-excitation, we multiply for each dye the spectral profile of the excitation light source, the dichroic reflectance (i.e., 1 minus its transmittance, neglecting absorption) and $\varepsilon \times F_{\text{abs}}(\lambda)$ (Fig. 5.6b, bottom). Integration over λ shows that – under these conditions – EGFP is 1.3-fold more efficiently excited than FM4-64. Stated otherwise, the (intentional) cross-excitation is 43% (FM4-64) versus 57% (EGFP), so both fluorophores are excited with (roughly) equal efficiency.

On the *emission* side, to calculate bleed-through we proceed similarly by tracing back the transmitted fluorescence through both microscope detection arms. Hence, to calculate the contribution of each fluorophore to the ‘red’ and ‘green’ colour image we consecutively multiply their fluorescence emission spectra with ϕ and the transmission curve of the primary dichroic mirror, the transmission (for the ‘red’ channel) and reflection (for the ‘green’ channel) of the secondary dichroic mirror (Fig. 5.6a, inset), and, for each channel, the transmission curves of the respective emission bandpass filters. The corresponding curves are shown in Fig. 5.6c (top). Again, we neglected the transmission spectrum of the microscope intermediate optics as well as the spectral response of the detector, which we assume to be uniform in the wavelength range studied. The result is illustrated in the bottom panel of Fig. 5.6c, and integration over λ yields a 4% estimate of the contamination of the green-detection channel with FM4-64 signal and of less than 0.01% EGFP detected in the red colour channel.

Finally, the *total cross-talk* between the red and green channels is given by multiplying the excitation cross-talk and emission bleed-through and dividing through the sum of these products for both fluorophores (Oheim et al. 2007). In the specific case of 488-nm excitation and simultaneous dual-emission imaging of FM4-64 and EGFP, we obtain that 99.98% of the signal detected in the red channel comes from FM4-64 and 96.85% of the signal detected in the green channel results from EGFP.

Thus, from the spectral separability analysis we expect that both EGFP and FM4-64 largely dominate the green- and red-detection channels, respectively, with only negligible cross-talk.

To facilitate the comparison of colocalisation data across different studies and to evaluate the error of the colocalisation estimate, it should be good practice to explicitly state the amount of cross-talk between the different detection channels used. The spectral separability index defined here offers a convenient criterion for evaluating and comparing multicolour data sets (Oheim et al. 2007).

Box 5.2 Optical sectioning techniques to lower image background and increase image contrast

Confocal microscopy is a well-established optical sectioning technique that is based on the observation that a point source of excitation light (illumination pinhole) can be used to create a diffraction-limited focus in the specimen plane, which in turn corresponds to a confocal spot in the image plane. Thus, in-focus light at locations different from the illuminated spot as well as out-of-focus signal can be efficiently rejected by placing a small pinhole (roughly of the diameter of the Airy disc) in the confocal image plane. To create an image, the spot is scanned with respect to the specimen, in biological confocal microscopy typically by scanning the beam angle in the objective pupil. Although it (slightly) increases resolution and (substantially) reduces background, confocal microscopy is not particularly well suited for live-cell imaging, because – as most generated fluorescence is rejected at the confocal aperture – it makes very inefficient use of excitation photons.

Multiphoton excitation fluorescence (MPEF) microscopy is a laser-scanning technique as well. Here, the improved image contrast and background rejection are achieved by restricting the fluorescence excitation volume, rather than the fluorescence collection volume as in confocal microscopy. The technique is based on the near-simultaneous non-linear absorption of two or more photons that combine their energies to excite a fluorophore from the ground state to the first excited state. MPEF is restricted to a tiny volume near the focus, because high photon densities are required for the phenomenon of multiphoton absorption (one way to think about this is to realise that the trajectories of multiple photons must cross the excited molecule simultaneously). MPEF uses infrared light to excite ultraviolet (three-photon excited fluorescence) or visible (2PEF) fluorescence. This, together with the broad 2PEF absorption spectra (compared with one-photon excited fluorescence), and the availability of the entire visible-wavelength range for fluorescence detection, permits efficient filtering and facilitates multiband recordings.

Total internal reflection fluorescence microscopy (TIRFM) is a light-confinement technique that exploits the phenomenon of total internal reflection of a light (in most instances, a laser) beam at a dielectric interface to generate a thin (approximately $\lambda/5$), exponentially decaying evanescent field that skims the lower-refractive-index medium. This near-field perturbation can be used to create a near-surface fluorescence excitation. When cells are grown on the dielectric boundary (i.e. the glass–water interface) only fluorophores in a thin near-membrane space are excited, whereas the bulk of the cell is spared from fluorescence excitation and photobleaching. Owing to its extremely low background, evanescent-field microscopy is often used when studying single-fluorophore photodynamics. Because the image is restricted to a thin section, TIRFM is typically used in conjunction with epifluorescence excitation.

Deconvolution. Within the approximation of linear imaging theory, each point of the object can be described as a point-source of light that gives – depending on its intensity and precise focal position – rise to a shifted and weighted copy of the point-spread function (PSF). Conversely, with knowledge of the experimental PSF, the information contained in a three-dimensional image stack can – in principle – be used to back-calculate the initial fluorophore distribution that produced the blurred diffraction-limited image. Although the reassignment of detected photons to their original location is – in principle – possible, the mathematical algorithms to solve this ‘inverse problem’ are fairly noise sensitive and are somewhat notorious in generating artefacts. In laboratory practice, three-dimensional image restauration by ‘deblurring’ is often outperformed by confocal imaging.

Reversible saturable optical fluorescence transition (RESOLFT) concepts. Contrary to what one might expect from the optical diffraction limit, fluorescence microscopy is in principle capable of unlimited resolution. The necessary elements are spatially structured illumination light and a non-linear dependence of the fluorescence emission rate on the illumination intensity. In saturated structured-illumination microscopy, the non-linearity arises from saturation of the excited state (Gustafsson 2005). The diffraction barrier has equally been broken by a saturated depletion of the marker’s fluorescent state by stimulated emission (Willig et al. 2006), but this approach requires picosecond laser pulses of gigawatt per square centimetre intensity. With use of much smaller intensities, subdiffraction resolution can be achieved from reversible photoswitching of a marker protein between a fluorescence-activated and a non-activated state, whereby one of the transitions is accomplished by means of a spatial intensity distribution featuring a zero (Betzig et al. 2006; Hofmann et al. 2005).

Section 5.2 revisits these examples to review different semiquantitative (colour merging, Sect. 5.2.1), pixel-based (Sect. 5.2.2), and object-based colocalisation estimates (Sect. 5.2.3) and discusses their performance. Box 5.3 extends the calculation of colocalisation coefficients to fluorophore abundance maps rather than fluorescence images. These maps are generated as a result of spectral imaging and linear unmixing (SILU) techniques in which the presence and relative contribution of fluorescent probes are analysed from a set of spectral images that is overdetermined, i.e., contains more planes than the sample contains fluorophores. We have recently introduced a variant of this technique specifically adapted for classifying resolution-limited point objects containing multiple fluorophores in live cells (Nadrigny et al. 2006).

Box 5.3 Multispectral and hyperspectral imaging

In addition to sequential or synchronous multiband recordings, many commercial laser scanning microscopes now permit multispectral or ‘hyper’-spectral detection. Spectral detectors are based on a dispersion element (prism, grating) and the parallel detection of a range of wavelength, either on a linear photodiode array (Zeiss) or on an arrangement of multiple photomultiplier tubes with movable entry slits (Leica). These instruments generate a flexibility that filter-based multichannel acquisition cannot offer. Spectral imaging devices have the advantage over earlier integrative (photometric) devices of providing – for each pixel – spectral and localisation information in addition to fluorescence intensities.

Because microscope images are diffraction-limited, neighbouring pixels of fluorescent objects are not independent; therefore, *object-based* approaches to quantify colocalisation can take into account a priori knowledge of the imaged object. An advantage of such object-based colocalisation analysis is that one can make use of additional information, e.g. the size and shape of the subcellular object under study, or of correlations between neighbouring pixels (Nadrigny et al. 2006).

When thinking in terms of multidimensional histograms (Sect. 5.2.3), we can view linear unmixing as a projection of each spectral pixel vector onto an orthonormal basis. Thus, instead of parameterising the spectral vector in terms of N fluorescence detection channels, its coordinates are given in terms of a set of k (pure) fluorophore vectors. Already with a surprisingly low number of spectrally overlapping detection bands (Neher and Neher 2004a) spectral imaging and linear unmixing permits fingerprinting the expression of spectrally overlapping fluorescent proteins on single secretory vesicles in the presence of a spectrally broad autofluorescence. By making use of statistical tools and the knowledge of the microscope’s PSF, this technique provides a robust alternative to error-prone dual-colour or triple-colour colocalisation studies in live cells (Nadrigny et al. 2006).

Most of the arguments used throughout this chapter rely on multiple-emission detection but symmetrically apply to experiments using multiple *excitation* wavelengths instead. We also note that although the optimal separation of fluorophore signal often requires both multiple-excitation *and* multiple-emission fluorescence imaging, we focus here on multiple-emission detection.

5.1.1 One Fluorophore, One Image?

Multicolour displays showing overlaid multichannel fluorescence images are increasingly being used in the cell and neurobiological literature to illustrate

molecular colocalisation and interaction. It is generally assumed that one fluorescence channel contains a specific signal, exclusively related to one fluorophore, and that images are comparable among different acquisition channels. Figure legends will typically read ‘**a** Confocal fluorescence images of a ... cell coexpressing a molecule X – enhanced-green fluorescent protein (EGFP) chimera (*top*), and protein Y fused to monomeric red fluorescent protein (mRFP, *bottom*). **b** Time series of EGFP (*top*) and mRFP images (*bottom*) reveals an increase in colocalisation after stimulation. **c** Pseudocolour overlay of EGFP and mRFP images. Note the increase in yellow indicating colocalisation (*arrowheads*)...’ or similar. Often, the precise experimental conditions (illumination, filter and detection settings, fluorophore variants used, etc.) are not very explicit and controls are omitted. The critical evaluation of colocalisation data requires more information than is often given. The major problems encountered with quantitative multicolour microscopy are well identified. Their relative importance, however, can vary from one microscope to another, from one experiment to another, and probably even from one batch of cells to another, depending, e.g., on the level of protein expression, autofluorescence in the preparation, or detector noise. For each combination of fluorophores imaged, it is important to quantify to what degree the different detection bands really contain independent and fluorophore-specific information. Also, although it might appear tedious and time-consuming, understanding the physical limitations of what can be achieved with a given combination of fluorophores, filters, and optical components is a useful exercise that lays the grounds for sensible instrument use. We stress this point specifically having the engineers and researchers in mind who are responsible for and run shared facilities and imaging platforms and can guide less experienced users to make judicious choices.

5.1.1.1 Spectral Overlap

Organic fluorophores typically display broad absorption bands that lead to considerable *cross-excitation*. Cross-excitation quantifies the amount of (usually unwanted²) excitation of fluorophores other than the one to be excited by this wavelength band. On the emission side, the problem is typically called *bleed-through* and relates to the amount of fluorescence that originates from other fluorophores detected in the fluorescence channel designed to view one specific fluorophore. Often, it is accentuated over cross-excitation because fluorescence tails off into the red owing to the decay into higher vibrational levels of the S₁ state and thermalisation of the excess vibrational energy, solvent effects, excited-state reactions, complex formation, or energy transfer. The total cross-talk will be proportional to the product of cross-excitation and bleed-through (Box 5.1).

² Special cases in which excitation cross-talk and emission bleed-through are not only tolerated but intentionally wanted are dual-colour emission detection with simultaneous excitation of two dyes emitting in different fluorescence bands, or dual-colour excitation with single-emission detection.

The ever-increasing generation of new fluorescent protein colour variants (reviewed in Shaner et al. 2005) and the expanding family of genetically encoded indicators (Griesbeck 2004) have not removed but rather accentuated the problem of fluorophore separation in multicolour fluorescence microscopy. Although a broader range of monomeric fluorescent proteins is becoming available, the choice of spectrally well separated variants is still very restricted. Also, for each new fusion protein and expression system, the specific targeting and lack of retention in the endoplasmic reticulum must be verified individually. For example, Hirrlinger et al. (2005) recently demonstrated that the formation of fluorescent precipitates limits the use of the spectrally attractive red-emitting reef coral proteins in transgenic animals. Those fluorescent proteins that work best have considerable overlap and cannot be separated using specific filter sets (Nadrigny et al. 2006; Zimmermann 2005).

We display in Fig. 5.1a two synthetic in-focus fluorophore maps. True fluorophore locations are represented by cross hairs (green) and circles (red), respectively. To model image formation, we convolved this high-resolution fluorophore map with an (experimentally determined interpolated high-resolution) point-spread function (PSF) of an objective with a numerical aperture (NA) of 1.45 and resampled the resulting diffraction-limited image with a pixelated imaging detector (Fig. 5.1b). The resulting red and green images were low-pass-filtered ($1 \mu\text{m}^{-1}$) and the low-pass-filtered image was subtracted from the original image to remove high-frequency noise. The result was thresholded to exclude background, and binarised. We estimated the colocalisation in the red channel (index 1), by calculating the degree of overlap of the two binary masks of the dual-colour image relative to the red binary image squared (Lynch et al. 1991),

$$\rho_{\text{bin}} = \frac{\sum_{\forall(x,y)} w_1^*(x,y) \cdot w_2^*(x,y)}{\sum_{\forall(x,y)} [w_1^*(x,y)]^2}, \quad (5.1a)$$

where

$$w_j^*(x,y) = \begin{cases} 255 & \text{if } w_1(x,y) \geq t_j \\ 0 & \text{else} \end{cases}, \quad (5.1b)$$

and the sum runs over all pixels (x,y) . $\frac{1}{255} \sum w_1^*(x,y)$ is the number of pixels above a threshold t_1 . We chose $t_1=t_2$ but the threshold levels for the red (index 1) and green (index 2) channels can (in principle) be chosen independently. $w_1(x,y)$ and $w_2(x,y)$ are the pixel values of the red and green images, respectively. ρ_{bin} measures the fraction of pixels on the green binary image that are equally present on the red binary image, relative to the total area of red pixels. We chose the somewhat bulky notation to allow for later generalisation (see below).

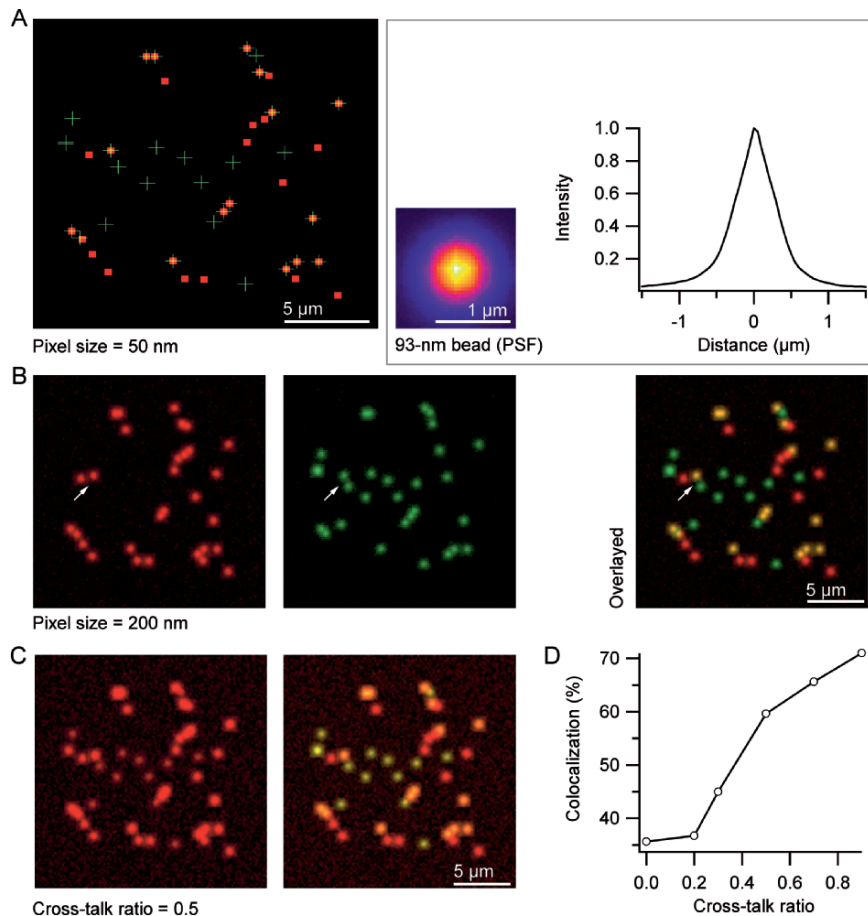


Fig. 5.1 Influence of cross-talk on colocalisation determination. **a** Artificially generated in-focus dual-colour images. To generate synthetic red and green high-resolution matrices 30 100-nm-diameter ‘fluorophores’ of each colour were placed on a grid of 50 nm. Red squares and green cross hairs indicate the ‘true’ particle positions. The actual degree of colocalisation was set as 50%, i.e. 15 particles colocalised, indicated by the overlap of both indicators, and the others were randomly distributed. Both high-resolution matrices were sequentially convolved with the experimental point-spread function (PSF), sampled by a low-resolution matrix with a pixel size of 200 nm, and shot noise was added to each pixel of the low-resolution matrix following a Poisson process. *Inset:* ‘High-resolution’ PSF. The experimental PSF determined by imaging a 93-nm fluorescent bead with an oil-immersion objective with a numerical aperture of 1.45 was radially averaged, interpolated, and resampled on a 50-nm grid. The line profile shows a linear cross-section of the interpolated in-focus PSF. **b** Green- and red-channel images and their pseudocolour overlap in the absence of spectral cross-talk. **c** Introduction of cross-talk. For clarity, only the cross-talk from the green channel into the red channel is evaluated. The cross-talk ratio is the amount of green fluorescence signal added to the red channel. An example (cross-talk ratio 0.5) is shown. **d** Increasing cross-talk adds a false colocalisation that can largely outnumber the ‘true’ amount of colocalisation. Colocalisation of 36% was estimated from the cross-talk-free fluorescent image pair using an object-based algorithm (see text for details)

Colocalisation in the green channel is estimated similarly, by dividing through $\Sigma[w_2^*(x,y)]^2$ instead. Owing to its use of binary image masks ρ_{bin} underestimates the true amount of colocalisation (36 vs. 50%), because even for a perfect match the added noise makes it impossible to delineate the real shape of the object. Thresholding favours the selection of high-intensity pixels, so the true particle size is underestimated when binarising the images and so is ρ_{bin} . See Sect. 5.2 for alternative descriptors of colocalisation.

What happens if we increase the cross-talk between both images? Figure 5.1c displays the red- and green-channel images and their pseudocolour overlay that result when increasing the fraction of the ‘green’ image leaking into the ‘red’ image. Whereas ρ_{bin} found 36% colocalisation on the original image pair, increasing the cross-talk ratio adds a false apparent colocalisation that can largely outnumber the true amount of overlap (Fig. 5.1d).

5.1.1.2 Low Signal

In order to provide meaningful estimates for fluorophore colocalisation, the fluorescence signal has to stick out of the image noise. In live-cell imaging, the sensitivity of the sample to high-intensity illumination (photodamage) and the loss of signal upon prolonged fluorophore excitation (photobleaching) often prescribe low excitation intensities. The resulting lower signal as well as the intrinsically dimmer fluorescence of fluorescent proteins (when compared with the commonly used organic fluorophores) requires additional precaution as to the interpretation of multicolour images. It might even be necessary to go back to fixed samples and use antibodies against the fluorescent proteins used so as to amplify the detectable signal above the noise level of the detector, however at the expense of losing quantitative intensity information (Martinez-Arca et al. 2003). Figure 5.2a shows, for the same image pair as shown previously, the effect of increasing the noise relative to a fixed signal in the green channel. The ‘red’ image is always the same, and we have assumed zero cross-talk between the two channels. Figure 5.2b displays the evolution of ρ_{bin} when the ‘green’ image fades away in the image noise. When always using the same fractional intensity for thresholding, the colocalisation becomes less and less apparent with increasing image noise, because fewer and fewer pixels remain after binarisation. However, other measures of colocalisation (Sect. 5.2) produce a different and even the opposite result. Median filtering (Demandolx and Davoust 1997) and deconvolution (Landmann 2002; Li et al. 2004) are two techniques that enhance the signal-to-noise ratio and colocalisation detection (not shown).

5.1.1.3 Three-Dimensional Spatial Resolution

Do two objects truly colocalise or do their images simply blur one into the other because the image resolution is low? Diffraction blurs the three-dimensional image

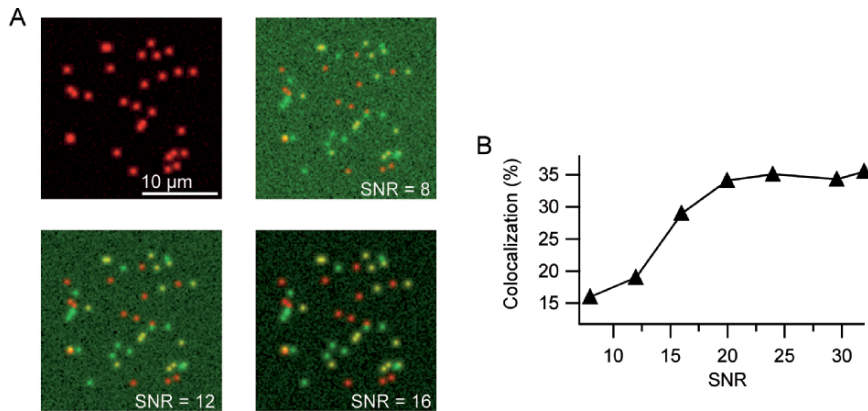


Fig. 5.2 Effect of decreasing the signal-to-noise ratio (SNR) in the green channel on colocalisation estimates. The ‘red’ image is always the same. In contrast, the noise was increased in the green channel for a constant signal of 500 counts. **a** Superimposed images of red- and green-channel images with different SNR levels as indicated. **b** Colocalisation is underestimated at low SNR. The amount of ‘true’ colocalisation in the absence of image noise is about 35% when using the object-based descriptor (Eq. 5.1) for estimating colocalisation. A minimal SNR is required to obtain reliable colocalisation estimates

of the object. In focus, subresolution objects appear with an apparent size much bigger than the true biological object given by the Airy disc, i.e. the in-focus plane of the three-dimensional PSF of the microscope (Fig. 5.1a, inset). Also, the microscope spatial resolution is not isotropic but is degraded along the microscope optical axis. Together with chromatic aberrations, diffraction results in spreading out a point object on the microscopic image, thereby creating a false apparent overlap between the images of proximal but not colocalised objects.

Defocus

Until now, we have assumed that all objects were located in focus ($z=0$) and the microscope had a perfect optical sectioning capacity. However, the objective will collect fluorescence from objects located above and below the nominal focal plane. These objects will contribute not with their in-focus image but with their respective (blurred) off-focus plane of the PSF. The spread of signal across multiple optical sections presents a significant source of false-positive artefact in the measurement of colocalisation (Fig. 5.3). To examine the effect of out-of-focus fluorescence on the colocalisation estimate, we moved the synthetic point objects to a random off-focus position drawn from a Gaussian distribution with mean d_z and the width given by the approximately $1.9\text{ }\mu\text{m}$ effective depth of field of a NA-1.45 objective. Figure 5.3 shows an in-focus fluorescence image pair, along with the corresponding

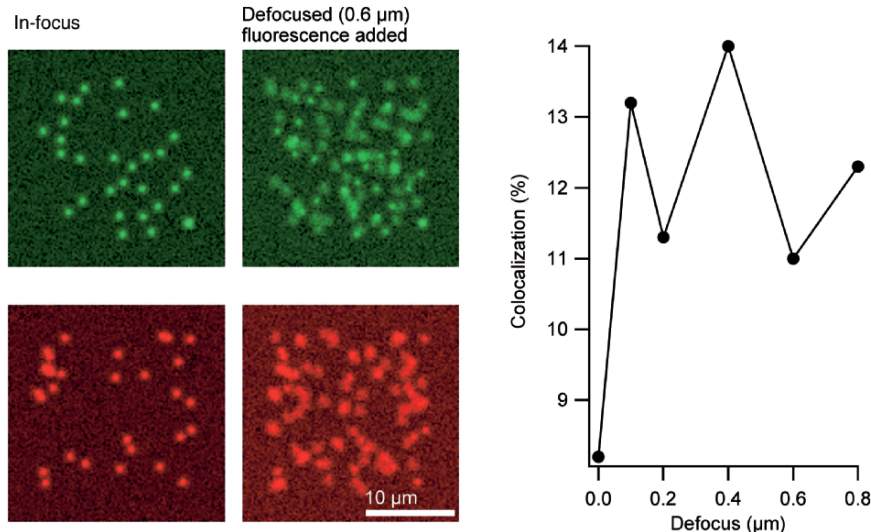


Fig. 5.3 Defocus results in false-positive colocalisation. Randomly distributed fluorophores were created for both channels. The colocalisation is low for the in-focus image pair, consistent with the small amount of random overlap resulting from the overlap of Airy patterns of proximal particles in the red and green channels. Moving objects slightly out of focus increases the apparent colocalisation and produces false positives (see text for details)

image in which we randomly introduced a mean defocus of $0.6\mu\text{m}$ in both image channels. We equally plot the evolution of ρ_{bin} when increasing defocus from zero to $0.1, 0.2, 0.4, 0.6$, or $0.8\mu\text{m}$. The amount of false-positive colocalisation resulting from overlapping Airy patterns for $dz=0$, and the effect resulting from the superposition of spatially unrelated signal give rise to an increasing false-positive colocalisation. Wide-field microscopy is only little suited for colocalisation analysis, because it suffers from out-of-focus blur. Image restoration by deconvolution can – in part – compensate for this problem, but is very sensitive to image noise and can generate bright pixels or grainy artefacts that are mistaken for fluorescent objects (Landmann 2002).

Lateral Resolution

The impact of lateral resolution on the apparent colocalisation of in-focus objects is illustrated in Fig. 5.4. We investigated this effect by placing red particles of $2r_1=100\text{-nm}$ diameter and green particles of increasing size $2r_2$ randomly in the object plane, respecting their mutual size exclusion, i.e. the interparticle distance is r_1+r_2 or bigger. For object sizes below or close to the optical resolution, the estimated false-positive colocalisation is low and roughly constant. With increasing

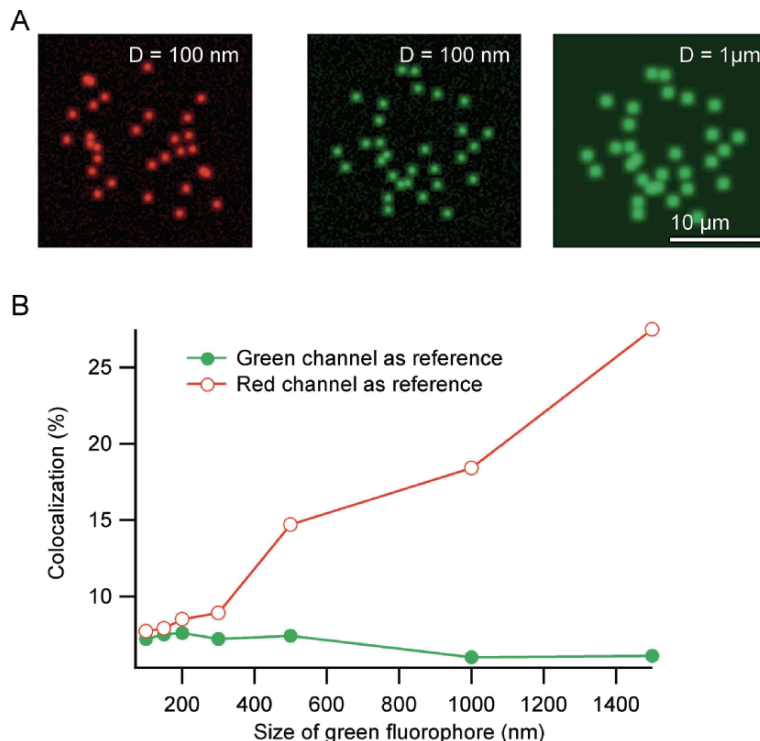


Fig. 5.4 The object size affects the colocalisation estimate. **a** Thirty red and green particles of 100-nm size each were created and randomly distributed in focus, respecting their mutual size exclusion, i.e. no two particle centres could get any closer than $r_{\text{red}} + r_{\text{green}}$, here 200 nm. The images were then blurred by convolution with the experimental PSF, Poisson noise was added, and the colocalisation was estimated as before. We then increased the diameter of green objects while keeping the red object size constant at 100 nm. The *leftmost panel* shows an example for 1-μm object size. **b** The size with which objects appear on fluorescence images is of critical importance in cases involving objects of near-resolution size. Evolution of the colocalisation estimate when using the red or the green channel as a reference (cf. Eq. 5.1a). The (false) apparent colocalisation rises with particle size in the red channel, because the number of pixels in which red and green overlap increases (owing to the bigger and bigger size of the green objects) while always dividing through a constant area of red pixels. Not the almost constant colocalisation estimate for particles with a size below or close to the optical resolution limit. In contrast, the colocalisation estimate is nearly constant when dividing the green and red overlap area by the concomitantly rising total area of green pixels. The slight drop results from the fact that the blurred edge creating the false overlap roughly grows as r_{green} , whereas the reference area grows as r_{green}^2

object size, ρ_{bin} (relative to the bigger-particle green image) slightly decreases, because the boundary effect becomes less and less prominent relative to the increasing green pixel area. As expected from the asymmetric three-dimensional resolution, ρ_{bin} is more sensitive to the axial than to the lateral resolution.

5.1.1.4 Non-rejected Background: Autofluorescence, Non-specific Protein Targeting, and Transmitted Excitation Light

Background is caused by electronic offset (Oshiro and Moomaw 2003), stray light, and blur from a specifically labelled or autofluorescent part of the object (Sheppard et al. 1995). Inefficient spectral filtering of ambient light or transmitted spurious excitation light can obscure faint signals too. Unfortunately, with sufficiently sensitive detection, virtually all cells contain detectable autofluorescence and the usually sufficient filter contrast ratios (i.e. the relative intensity of transmitted vs. reflected light) become limiting. Also, with intense ultraviolet and low visible excitation, glass components (cover slip, objective lens, etc.) can produce a background autofluorescence. Testing different substrates and immersion oils and performing appropriate controls can help to identify and reduce background. Belonging to the same class of problems, a fusion protein may not be exclusively directed to its target organelle but may be retained in the endoplasmic reticulum or in cytoplasmic and membranous locations as well. For example, appreciable amounts of the vesicle-associated membrane protein 2 (VAMP2) are found on the plasma membrane after expression of a fluorescent protein chimera (Nadrigny et al. 2006). Although these backgrounds have fundamentally different origins, they have in common that they produce a diffuse apparent spatial overlap outside areas of true colocalisation in a way similar to the effect observed at a low signal-to-noise ratio (Fig. 5.3). Figure 5.5 shows that spurious background impairs image quality in two respects. First, it buries low-intensity signal and obscures image detail (Fig. 5.5a). Second, it affects resolution, as the high-spatial-frequency image components are generally of less intensity than the low-frequency ones. Therefore, colocalisation analysis critically depends on the background level (Fig. 5.5b), which must be reduced to a minimum, e.g. by the use of optical sectioning techniques that reduce the fluorescence excitation or readout volume (Box 5.2).

5.1.1.5 Ultradeep Imaging in Intact Tissue with Two-Photon-Excitation Fluorescence Microscopy

Genetically encoded probes permit the targeting and tagging of subpopulations of cells *in vivo* and are emerging as a powerful tool for imaging cellular and molecular biological function in the living animal (reviewed in Miyawaki 2005). 2PEF imaging usually offers a more efficient filtering than its one-photon counterpart, owing to the large spectral separation between the infrared excitation and visible fluorescence, but this advantage is to some extent compensated for by the high instantaneous intensities required for efficient *in vivo* 2PEF and the faint fluorescent signals emerging from deep tissue sections. Also, *in vivo* 2PEF microscopy of optically thick tissue sections is associated with a number of problems that stem from the increasing diffusion (i.e. spatial redistribution) of photons with greater imaging depths (Beaurepaire and Mertz 2002; Oheim et al. 2001) and affect colocalisation measurements.

For example, with increasing depth, the scattering of excitation photons prohibits the formation of a tight focus, thereby degrading the resolution (through filtering out

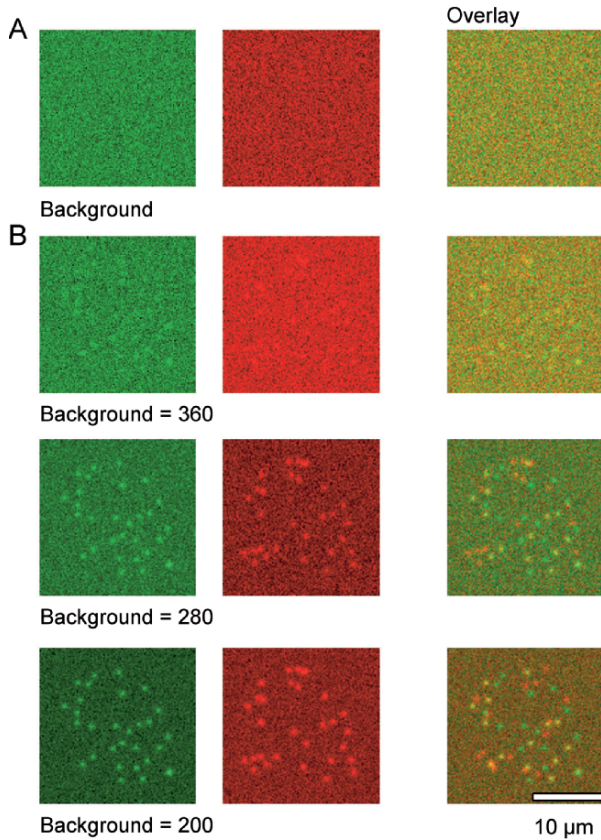


Fig. 5.5 Non-rejected background. **a** In the extreme case of colour-merging green- and red-colour background, the resulting overlap image displays a homogeneous yellow signal – featureless nearly perfect colocalisation. **b** To investigate the impact of non-rejected image background on the colocalisation estimate, the fluorophore intensity (useful signal) was kept constant at 500 counts, whereas the background level was chosen as indicated in the *leftmost panels*. Low background facilitates the detection of colocalisation

photons that travel at high NA) and reducing the signal (by decreasing the number of photons that arrive at the focal spot and contribute to 2PEF). Also, even when a detectable 2PEF is still generated at depths, fluorescence photons are scattered on their way to back the objective, so the collected fraction dwindles with increasing depth penetration, unless a high-NA large-field detector is used (Oheim et al. 2001). Finally, when compensating for these intensity losses by increasing the total laser power incident on the specimen, out-of-focus fluorescence and tissue autofluorescence are generated near the tissue surface. This is because the (diffuse) incident intensities are so high that the photon density in the unfocused pulsed beam is sufficiently high to generate out-of-focus 2PEF. This diffuse signal excited at the tissue surface is more efficiently collected and can attain the same order of magnitude and

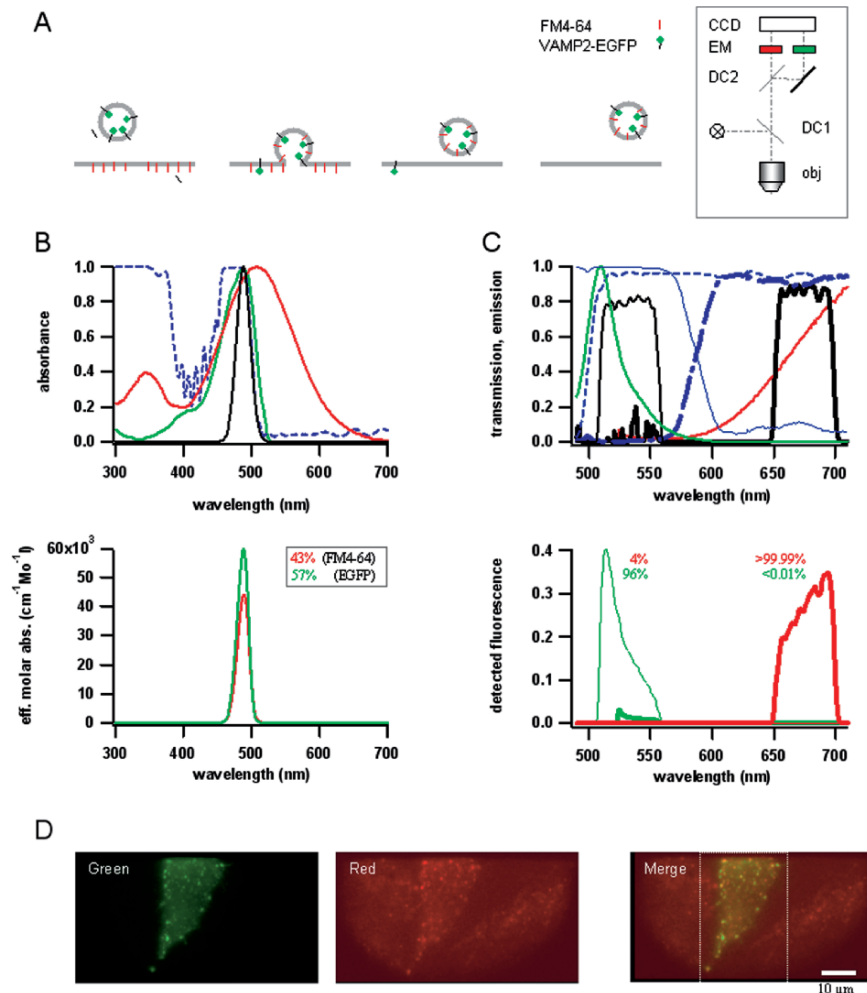


Fig. 5.6 Choosing appropriate filters for a given pair of fluorophores. **a** Endocytic uptake of the lipid membrane dye FM4-64 into secretory granules expressing a fusion protein of enhanced green fluorescent protein and vesicle-associated membrane protein 2 (EGFP-VAMP2). Note that FM4-64 is fluorescent when inserted in lipid membranes but virtually non-fluorescent in aqueous solution, as represented by red sticks and black sticks, respectively. **Inset:** The microscope light path with a dual viewer (500DCLP primary and 590DCXR secondary dichroic, HQ535/50m and HQ675/50m emitters). *obj* objective, *DC1* dichroic mirror, *DC2* secondary dichroic mirror, *EM* emission filters, *CCD* charge-coupled-device camera. **b** **Top:** Normalised spectra of the excitation band used ($488t \pm 12 \text{ nm}$, solid black line) and the reflection curve of the dichroic mirror (500DCLP, dashed blue line) as well as the normalised absorption spectra of FM4-64 (red) and EGFP (green). **Bottom:** Product of the spectral excitation, dichroic reflectance, and molar extinction for FM4-64 (red) and EGFP (green), respectively. **Inset:** Numbers are the integral over wavelength, $d\lambda$. (Intentional) excitation cross-talk for 488-nm excitation is 43% (FM4-64) vs. 57% (EGFP), leading to roughly equal excitation of both dyes. **c** **Top:** Normalised emission spectra of FM4-64 (red) and EGFP (green), as well as the emission bandpass filters for their detection (thick black line and thin black line, respectively). **Blue lines**

obscure the faint collected in-focus signal from larger imaging depths (Oheim et al. 2001; Theer et al. 2003). In conclusion, for the same amount of physical colocalisation, the apparent measured colocalisation will vary with imaging depth.

5.1.2 A Practical Example of Dual-Band Detection

From the foregoing discussion it is clear that the quality of the colocalisation estimate critically depends on a variety of parameters. In practice, the ‘quality’ of the colocalisation measurement will depend on choosing appropriate combinations of dyes and filters in a given experimental situation, which requires knowledge about the level of autofluorescence in the sample and the sensitivity and spectral characteristics of the detector. Figure 5.6 shows a realistic experiment. We want to image the endocytic and exocytic dynamics of a defined subpopulation of secretory vesicles in cortical astrocytes, using a fluorescent marker of the styrylpyridinium dye family that is internalised upon endocytosis in an activity-dependent manner, and a monomeric fluorescent protein vesicle protein marker. A look at the available fluorescent probes suggests two possible combinations: (1) the use of the green fluorescent FM1-43 dye together with a monomeric red fluorescent protein (mRFP-1) chimera or (2) the (spectrally) inverse, i.e. the use of the red variant *N*-(3-triethylammoniumpropyl)-4-(6-(4-(diethylamino)phenyl)hexatrienyl)pyridinium dibromide (FM4-64) together with a green fluorescent protein construct (EGFP, pEGFP-N1, Clontech). When expressed in cells, the mRFP1–VAMP2 fusion protein produced a granular red fluorescence of spots; the size, dynamics, and response to intracellular calcium concentration elevations were compatible with secretory vesicles. Control experiments in which we expressed mRFP-1 displayed a clustered signal in front of the expected diffuse red cytoplasmic fluorescence (D. Li, F. Nadigny, J. Hirrlinger, P.G. Hirrlinger, N. Ropert, F. Kirchhoff, and M. Oheim, unpublished data). EGFP–VAMP2 did not show a comparable mistargeting, so we rather opted for the FM4-64/EGFP pair (Blazer-Yost et al. 2001; Jomphe et al. 2005; Sharp and Pogliano 1999; Shoji et al. 2006; Tyler et al. 2006).

FM4-64 belongs to the same family of dyes as FM1-43 and is non-fluorescent in water but increases its fluorescence quantum yield by more than 2 orders of

Fig. 5.6 (continued) are the transmission of the primary (*dashed blue line*) and secondary (*dot-dashed blue line*) dichroic mirror as well as the transmission of the latter (*solid blue line*), respectively. **Bottom:** Effective contribution of FM4-64 (*thick line*) and EGFP (*thin line*) to the fluorescence detected in the red and green channels, respectively. See Box 5.1 for details. **d** Epifluorescence images of three mouse cortical astrocytes in culture, labelled with FM4-64 taken in the configuration shown in **a**. The cell in the *middle* equally expresses VAMP2-EGFP. *Left:* ‘Green’-detection channel image (epi488|dic500|dic590|em535/50). *Middle:* ‘Red’-detection channel image (epi488|dic500|dic590|em675/50). Note the partial colocalisation in the pseudocolour overlay, *(right)*. The *boxed region* is analysed further in Fig. 5.12

magnitude upon insertion in lipid membranes (Brumback et al. 2004; Fig. 5.6a). Its peak excitation (558 nm) and emission (734 nm) are both redshifted (Table 5.1) compared with those of FM1-43 (Betz et al. 1996) owing to three double bonds linking the positively charged head and lipophilic tail group. Both EGFP and FM4-64 can be simultaneously and efficiently excited (with 99 and 93% of their peak absorption, respectively) with the quasimonochromatic (488 ± 12 -nm) excitation band of a TILL Polychrome II (Messler et al. 1996) without further excitation filtering (Fig. 5.6b, top). Simultaneous EGFP/FM4-64 excitation removes the need to change filter cubes between acquisitions and offers the possibility of a simultaneous side-by-side projection of the green and red images on the same imaging detector. We used a 500DCLP primary dichroic mirror to reflect the excitation light onto the sample and a custom dual-viewer device in the two detection arms of the microscope (Fig. 5.6c, bottom).

Figure 5.6d displays the dual-channel fluorescence image pair of a group of cortical astrocytes labelled with FM4-64 and transfected with a plasmid encoding VAMP2-EGFP. As only the cell in the centre is expressing the fusion protein, we can directly estimate the amount of cross-talk from the images. Hardly any fluorescence is seen on the green-detection channel in the two cells flanking the transfected cell in the centre. Indeed, no FM4-64 signal is contaminating the green-detection channel. A comparison of the single-spot fluorescence and intensity line profiles on the red-detection channel reveals little if any increased intensities in the EGFP-expressing cell relative to its neighbours, indicating that EGFP signal is excluded from the red-detection channel (not shown).

However, even when choosing fluorophores of comparable brightness $\epsilon\phi$ (Wessendorf and Brelje 1992), carefully balancing the detection efficiency, and avoiding spectral cross-talk, different (local) fluorophore concentrations can produce images of very different intensity that flaw colocalisation estimation. This is particularly a concern when fluorophore concentrations are unknown or only controlled in a very indirect manner, e.g. with acetoxyethyl ester loading or transfection (see Nadigny et al. 2006 for a critical discussion).

Also, for many combinations of fluorophores and fluorescent proteins, fluorescence overlap is unavoidable. It can be dealt with, to some extent, with narrowband detection – at the expense of the collected signal. Dual-excitation dual-emission protocols can help to accentuate the differences between fluorophores while maintaining a constant signal, but changing filter cubes between acquisitions slows down the acquisition rate. Dichroic mirrors with multiple reflection bands can be employed to extend this dual-colour scheme to experiments with several dyes that excite and emit at different wavelengths. However, such multiband filters have reduced band-pass transmission and broadened reflection bands, leading to greatly reduced emitted photon collection efficiencies. To avoid such losses, a microscope design that allocates spatially separate portions of the objective lens aperture to excitation and emission beams without using a conventional dichroic mirror has been proposed (Friedman et al. 2006).

Finally with the exception of a few well-established cases (e.g. 4',6-diamidino-2-phenylindole/fluorescein isothiocyanate/Texas Red), triple-band recordings of

three labels are not feasible, particularly when autofluorescence is present or when the signals are faint (see, however, Finley et al. 2001; Lowy 1995; Xia et al. 2006). Instead, spectral ‘oversampling’ by acquiring a small number of spectral images larger than the number of fluorophores present in the sample can be a simple yet effective means to discern overlapping fluorophores (Nadrigny et al. 2006; Neher and Neher 2004a; Zimmermann 2005). In this case, the colocalisation estimate is not calculated from the fluorescence images but rather is derived from an ‘unmixed’ fluorophore abundance map (Box 5.3).

5.2 Quantifying Colocalisation

With a set of (near-) independent fluorophore maps at hand the next step is to calculate their relative degree of spatial overlap. Different techniques for measuring colocalisation are available. Although a clear distinction is not always straightforward, we group the various approaches in two principal families, those that:

1. Analyse *single-pixel intensity values* over the entire image area or subregions
2. First *segment* the image *and then detect objects* and compare their area and/or intensity

Whereas the former approach considers the acquired data set as a $5N$ -dimensional vector [two lateral spatial dimensions (xy) plus one axial spatial dimension (z) plus time- plus N spectral dimensions] in which each pixel is treated as an independent element, the later approach identified objects and classifies them, by detecting fluorophore presence and colocalisation, and then tracks them over time. Both approaches have their distinctive advantages and drawbacks, but it is important to realise that they generally will not produce identical colocalisation estimates.

5.2.1 ‘Colour Merging’

Many published estimates of colocalisation are only qualitative and are based on an image-overlay method, i.e. the superposition of one fluorescence image, (pseudo-) coloured ‘green’ (Fig. 5.6d, left), on image two, coloured ‘red’ (Fig. 5.6, middle) to give ‘yellow’ (Fig. 5.6, right). A formally equivalent qualitative representation of the total overlap is obtained by subtracting one component image from the other (Akner et al. 1991; Oheim et al. 1999).

Colour merging is implemented in many commercial imaging software packages. The evaluation of the degree of colocalisation is generally visual-based and therefore prone to error and bias, as the ‘amount of yellow’ depends on the brightness of the merged images, the monitor settings, as well as the viewer’s perception. Also, the displayed

image triplet only reports one anecdotic observation and does not account for the variance in colocalisation observed for an ensemble of image pairs studied.

5.2.1.1 The Dos and Don'ts for Measuring Colocalisation

Any colocalisation measurement should:

- Use maximally independent image pairs (Sect. 5.1), and quantify the degree of cross-talk that is present (and tolerated) in the experiment.
- Define the parameter used for measuring co-localisation.
- Report a distribution of this parameter for a statistically significant sample of objects, cells, fields of view, etc., rather than a single value.
- Normalise the reported degree of colocalisation to some commonly accessible reference standard, e.g. multispectral subresolution beads, or dual-colour conjugates of nanocrystals. In practice, the absence of this type of normalisation is one of the main difficulties that prevents that data from the literature being directly compared.
- Show the same type of analysis for a negative control, i.e., an experiment, in which the same pair of fluorophores is directed to two molecules or subcellular compartments that can be assumed to be distinct. Sometimes, such negative controls have been performed by rotating one colour-channel image by 90° with respect to the other and recalculating the amount of colocalisation. A better strategy that takes into account the object size and density as well as the cross-talk is to place randomly the same number of solid (i.e. finite-extend) objects, convolved with the experimental PSF, on an area equal to the available area on the colocalisation image studied, and then to recalculate the colocalisation estimate over 30 trials. This procedure inherently takes into account the non-zero random overlap (Fig. 5.4b) resulting from the diffraction-limited resolution as well as trial-to-trial variability. In order to be called ‘colocalised’, the experimental distribution should be statistically different from the control distribution that gives a lower bound of meaningless (random) colocalisation.
- Report a positive control, i.e. an experiment, in which the same pair of fluorophores labels the same molecule or subcellular compartment. Again, and depending on the precise parameter calculated (see below), the calculated colocalisation estimate will not be 100%, even in the case of perfect spatial overlap. Alternatively, a synthetic image can be generated, convolved with the PSF, and image noise added as shown earlier. The resulting parameter distribution defines an upper bound and – together with the negative control – identifies the interval for meaningful colocalisation estimates.
- Use statistical tests to decide if the observed colocalisation distribution differs from a random (or perfect) control situation.

The result will probably be one of *partial colocalisation* (Fig. 5.6d). Even careful controls cannot remove the ambiguity of how to interpret the calculated parameter. Absolute values of colocalisation are always instrument-dependent. The best one can hope for is to arrive at statements like ‘the measured amount of colocalisation was

significantly higher than what is expected from a random distribution of the same organelles/molecules/...’ or ‘however, not all molecules X colocalised with Y, as the measured colocalisation significantly differed from a perfect match...’. A consistent yet laborious strategy to circumvent such problems is to compare the amount of colocalisation between the molecule of interest and different (spectrally identical) markers, e.g. the fluorescent proteins fused to different proteins, and to report their relative degree of colocalisation. When the different constructs are of about the same size and are expressed under the control of the same promoter, this procedure can also, at least in part, compensate for artefacts resulting from protein overexpression.

5.2.2 Pixel-Based Techniques

A more rigorous quantification of the overlap region than the colour merging method requires the simultaneous evaluation of spatial and intensity data in both colour channels (Garcia Peñarrubia et al. 2005). The first aspect, looking for the spatial correspondence of data pixels, is easily achieved once the two images have been brought in register. This can be done with the help of subresolution multiple-emission point sources as reference points (e.g. MultiSpeck™ beads, Invitrogen) as positive controls for true colocalisation at different image locations. If the sensitivity of the detector used is too low, imaging larger (and brighter) beads that contain one fluorophore on their surface and are labelled throughout with the other are a good choice. Next, after images have been aligned and corrections for chromatic aberrations have been made (Kozubek and Matula 2000) the spatial correspondence is investigated by collecting all pixel-intensity data pairs at corresponding x,y locations and plotting them as a two-dimensional histogram. In Figs. 5.7–5.11 we plot this type of analysis for the synthetically generated images previously shown. Figure 5.12 displays the scatterplot for the FM4-64/EGFP double-labelled cell shown in Fig. 5.6d.

5.2.2.1 Scatterplots, Multidimensional Histograms, and Spectral Angle Matching

The result is a two-dimensional scatterplot (or ‘cytofluorogram’; Fig. 5.7), where the axes represent the intensity ranges of the two images and one point is one pixel. The point density in the pixel cloud is indicative of the frequencies of the intensity data pairs. In a noise-free, background-subtracted image, pixels containing pure fluorophores populate the paraxial regions (Fig. 5.7, top right). Extended, multifluorescent objects with their pixels having roughly a fixed intensity ratio between both channels result in a diagonal pixel cloud, the thickness of which reflects noise contributions of background noise. As noise-reduction techniques, low-pass and median filtering as well as image deconvolution can help to thin down the cloud, particularly at the low-intensity end (Landmann 2002). Cross-talk between detection channels brings the lobes of pure and mixed pixels closer to each other.

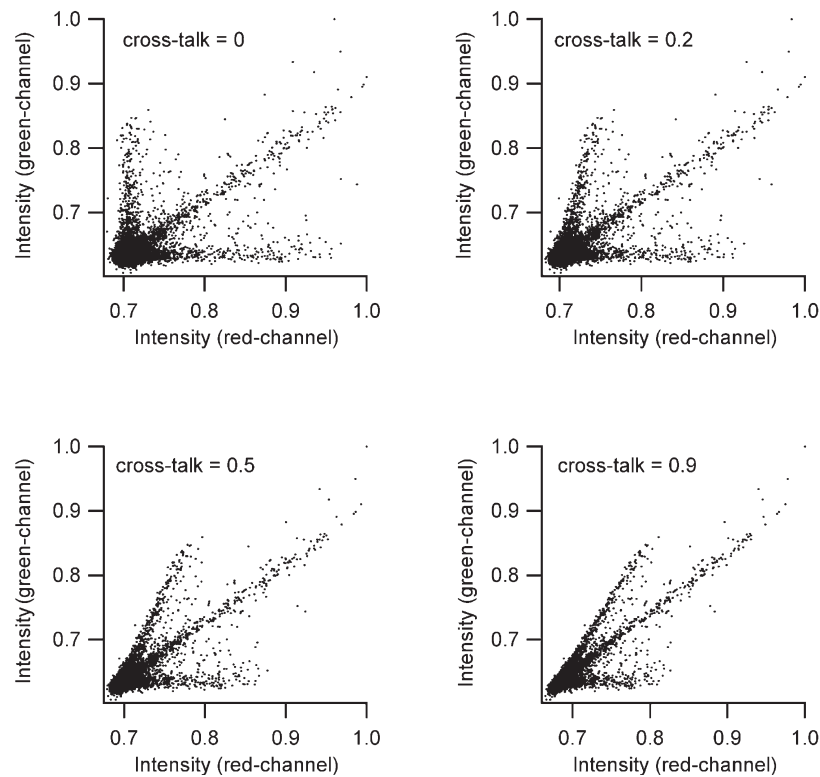


Fig. 5.7 Pixel analysis for the influence of cross-talk on colocalisation determination. Each image pixel is represented as a spot on the two-dimensional histogram. Axes are normalised to maximal intensity in each component image. The graphs illustrate the impact of increasing the cross-talk from the green into the red channel for the same images as shown in Fig. 5.1. Pure fluorescent species are found in paraxial regions, whereas mixed pixels that appear at roughly equal intensity on both component images populate the diagonal. Brightest pixels are located in the distant corners. Cross-talk brings the lobes representing pure pixels closer to the region of mixed pixels, reducing the spectral angle between ‘pure’ and mixed pixels, thereby increasing the apparent colocalisation

Therefore, the second (and trickier) part involves the determination of the zone of the scatterplot in which ‘true’ colocalisation occurs. Only pixels inside these boundaries will be considered for the colocalisation analysis. In practice, rectangular or conical colocalisation areas are the most frequent selections. The intensity-based scatterplot analysis is frequent in photometric devices like flow cytometers and cell counters (where labelled cells are relatively easily distinguished from autofluorescent and unlabeled ones and one cell analysed gives rise to one point on the scatterplot). In microscopic imaging, heterogeneity occurs at the subcellular level and the segmentation and interpretation of scatterplots is less straightforward (Garcia Peñarrubia et al. 2005). The lack of general criteria to select an area of colocalisation on the scatterplot makes this task both difficult and ambiguous. Typically, selecting

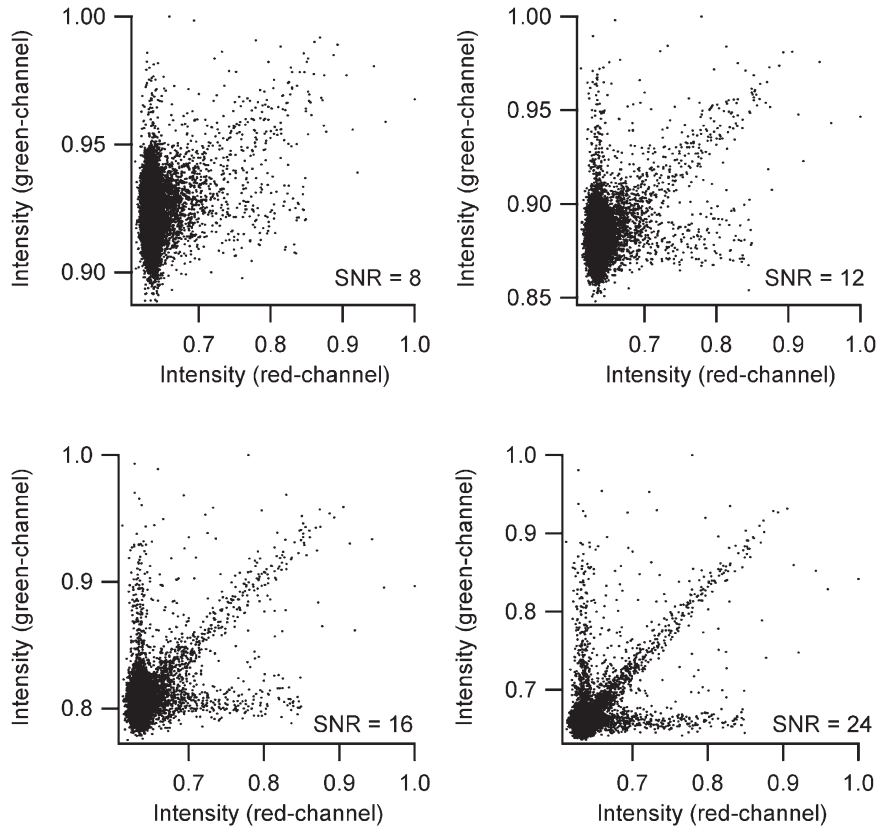


Fig. 5.8 Pixel analysis of the effect of the SNR on the colocalisation estimation. The graphs illustrate the impact of decreasing the SNR in the green channel, as shown on the images in Fig. 5.2. The red-channel image is always constant. Decreasing the SNR in the green-detection channel produces an increasingly featureless pixel cloud. The number of pixels that can be extracted and used for the calculation of the colocalisation coefficient becomes lower. With decreasing SNR, the interpretation and segmentation of scatterplots becomes less and less straightforward

a scatterplot region is done by thresholding each component image individually, which again leaves room for user-bias. One way to interactively control the choice is to produce a binary mask on the analysed images so that the user can see the position on the image of the selected pixel and compare this choice with some a priori knowledge about the fluorescent label, e.g. object size, shape, or localisation relative to other visible subcellular structures.

The *multidimensional histogram* extends the scatterplot type of analysis to data sets containing more than two fluorophores and prepares the ground for SILU approaches (Box 5.3). Each pixel (x,y) is represented by a spectral vector:

$$\mathbf{w}(x,y) = [w_1(x,y), w_2(x,y), \dots, w_N(x,y)]^T. \quad (5.2a)$$

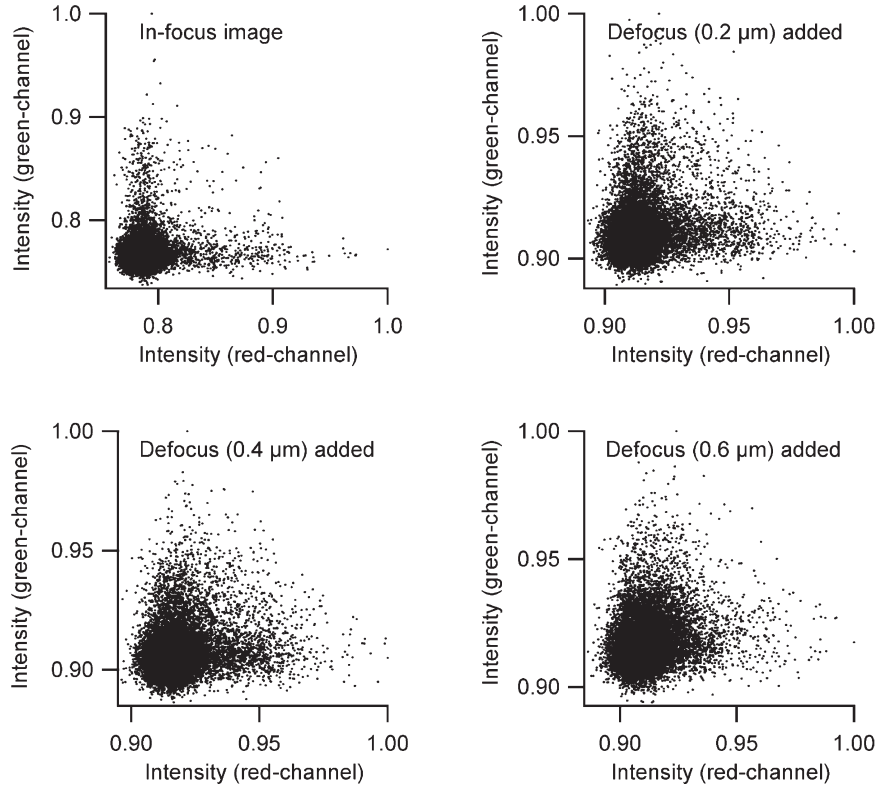


Fig. 5.9 Pixel analysis of the effect of out-of-focus fluorescence. The graphs illustrate the impact of moving some of the red and green objects out of focus, as shown in Fig. 5.3. On the two-dimensional scattergram, the initially well-separated lobes of unrelated fluorescent spots of the red and green component images increasingly merge upon addition of defocus. The spectral angle decreases and more and more pixels populate the diagonal and are (falsely) mistaken for colocalising pixels

Its N components w_i denote the intensity of pixel (x,y) in each detection band. For a more convenient notation, we replace the two-dimensional pixel index (x,y) by a running index $i \in [1, \dots, n]$, where $n = x_{\max} \cdot Y_{\max}$,

$$\mathbf{w}(i) = [w_1(i), w_2(i), \dots, w_N(i)]^T \quad (5.2b)$$

In the case of zero cross-talk between the N detection channels, the N unit vectors form an orthonormal basis that spans the N -dimensional fluorophore space. Otherwise, the projection of $\mathbf{w}(i)$ on the pure fluorophore vectors defines a k -dimensional subspace ($N > k$, linear unmixing). Each pixel is represented by a vector and the projection on the axes measures the relative amount of fluorophore(s) present in that pixel. As in the two-dimensional case, above, the tricky part consists of delineating the N -dimensional

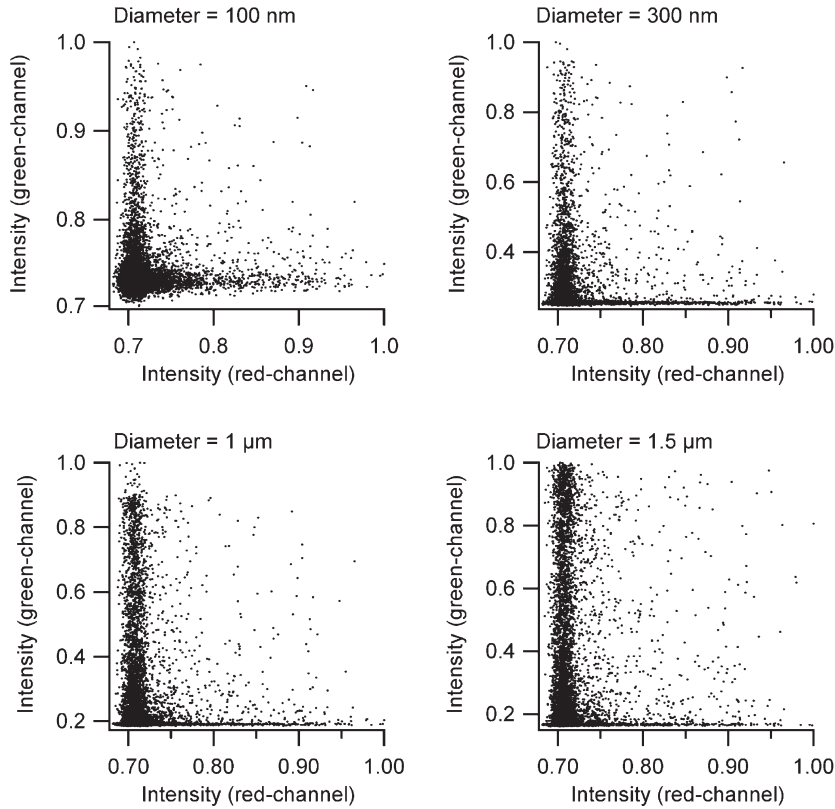


Fig. 5.10 Pixel analysis of the influence of the change in the object size on the colocalisation estimate. Diffraction adds a blur to the single-particle image that creates a false-positive colocalisation, even in the case of only proximal, non-overlapping (i.e. in-focus) particles. The graphs illustrate the impact of increasing the physical size of the green objects, as shown in Fig. 5.4. Diameters specify the ‘true’ physical size of the green particles before convolution with the PSF and addition of noise. Red particles always measured 100 nm in diameter. As green particles get bigger and bigger, more and more green pixels (that correspond to the luminous centre of the spherical particles) populate the high-intensity end of the two-dimensional scattergram

volumes that identify pure or coexisting fluorophores. Therefore, a different and more intuitive strategy classifies pixels by measuring their spectral similarity, based on *spectral angle* mapping (SAM) (Kruse et al. 1993; for examples see Neteler et al. 2004; Shrestha et al. 2005) or by using statistical descriptors that test for outliers among the spectral vectors (Nadrigny et al. 2006). The spectral angle,

$$\theta_i = \arccos\left(\frac{\mathbf{w}(i) \cdot \mathbf{r}}{\|\mathbf{w}(i)\| \cdot \|\mathbf{r}\|}\right) = \arccos\left(\frac{\sum_{j=1}^N w_j r_j}{\sqrt{\sum_{j=1}^N w_j^2} \cdot \sqrt{\sum_{j=1}^N r_j^2}}\right), \quad (5.3)$$

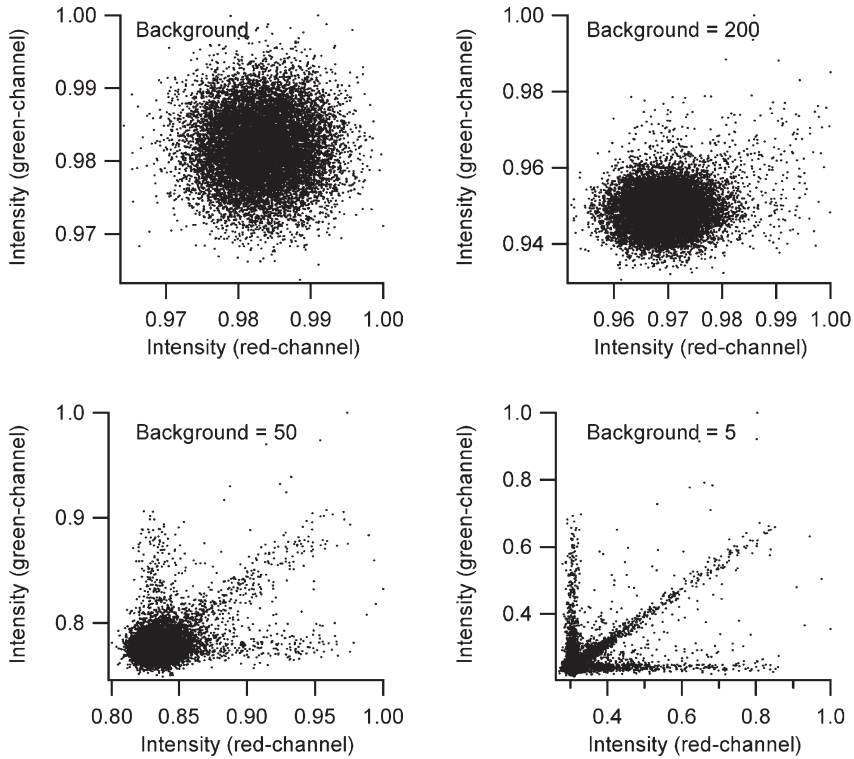


Fig. 5.11 Effect of non-rejected background on the two-dimensional scatterplot. The graphs illustrate the impact of adding a homogenous image background to the green image (mean intensity indicated) on the colocalisation estimate. The corresponding images are shown in Fig. 5.5. *Top left:* Two-dimensional histogram for pure red and green background images. *From top right to bottom right:* Effect of decreasing the relative contribution of a constant background. The peak signal of the ‘true’ signal was 500 counts. With decreasing background, the three-lobe signal (pure red, pure green, and colocalising pixels) gradually emerges from the centrosymmetric background scattergram

measures the resemblance of the pixel vector $\mathbf{w}(i)$ with a reference vector \mathbf{r} , which will typically represent a known fluorophore, e.g. cytoplasmically expressed EGFP. Since SAM compares only the spectral angle between pixels containing known fluorophores and pixels containing unknown (potentially colocalised) fluorophores and not the length of the vector, the method is fairly insensitive to intensity differences. Also, no a priori knowledge about the exact shape of $\mathbf{w}(i)$ is required, so SAM is useful in situations where strong autofluorescence is present. An intuitive way to represent colocalisation is to measure the average vector $\langle \mathbf{w}(i) \rangle_{\text{coloc}}$ from an image region (or control experiment) where colocalisation occurs and to compare this reference vector with each pixel vector \mathbf{w} . θ is then determined for each pixel i and the result is plotted as a pseudocolour map $\theta_i \in [0,1]$. This type of analysis bears resemblance to the classification problem in the satellite imaging and remote sensing literature (cf. multispectral and hyperspectral imaging).

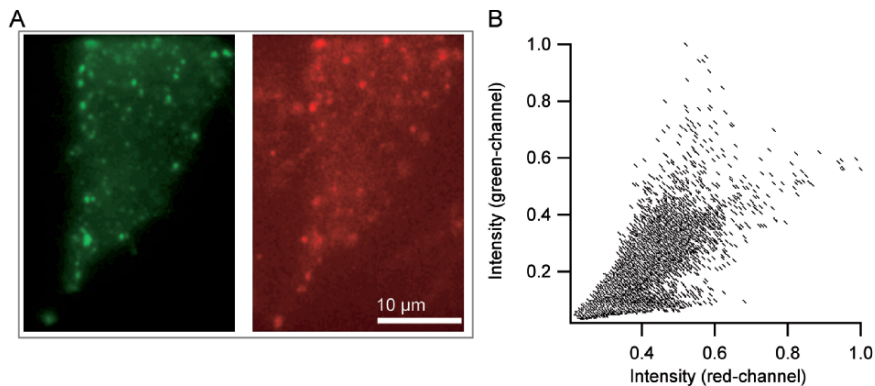


Fig. 5.12 Pixel analysis of the FM4-64/EGFP double-labelled astrocyte. **a** Excised region of interest taken from the centre of the dual-colour image shown in Fig. 5.6, showing a cortical astrocyte labelled with FM4-64 and expressing VAMP2-EGFP, viewed through the ‘red’ (HQ675/50 m) and ‘green’ (HQ535/50 m) microscope detection arms. See Box 5.1 for details. **b** Two-dimensional scattergram of the image pair shown in **a**. Three lobes can be distinguished in the pixel cloud. The lobe structure reveals that the intensity and contrast are higher in the green channel and that the signal-to-background and SNR are lower in the red-detection channel. The spectral angles apparent from the lobes are often misleading, owing to the non-uniform pixel density obscured by the finite symbol size.

5.2.2.2 Cross-Correlation Analyses: Pearson’s Correlation Coefficient and Overlap Coefficients

A different method that uses the information of all pixels as well but calculates the degree of correlation between the intensity grey values of the pixels in a dual-colour image is the estimate provided by Pearson’s correlation coefficient ρ_p (Manders et al. 1992, 1993). Pearson’s correlation coefficient is one of the standard measures in pattern recognition (Gonzales and Wintz 1987) for matching one image with another and provides information about the similarity of shape without regard to the average intensity of the signals in both component images. It is calculated for two component images 1 and 2 as

$$\rho_p = \frac{\sum_i^N [w_1(i) - \langle w_1 \rangle_{vi}] [w_2(i) - \langle w_2 \rangle_{vi}]}{\sqrt{\sum_i^N [w_1(i) - \langle w_1 \rangle_{vi}]^2 \cdot \sum_i^N [w_2(i) - \langle w_2 \rangle_{vi}]^2}}, \quad (5.4a)$$

where $w_j(i)$ and $\langle w_j \rangle$ represent the fluorescence intensity of each pixel i and the average over all pixels of the component image j , respectively. N is the total number of pixels in each image. ρ_p is formally and mathematically equivalent to the cross-correlation coefficient (Stauffer and Meyer 1997), in which fluorophore colocalisation is measured by

$$\rho_c = \frac{\frac{1}{N} \sum_i^N [w_1(i) - \langle w_1 \rangle_{\forall i}] [w_2(i) - \langle w_2 \rangle_{\forall i}]}{\sqrt{\frac{1}{N} \sum_i^N [w_1(i) - \langle w_1 \rangle_{\forall i}]^2} \sqrt{\frac{1}{N} \sum_i^N [w_2(i) - \langle w_2 \rangle_{\forall i}]^2}}. \quad (5.4b)$$

A tool for automating this process in ImageJ has been published (Rodgers 2002).

In this type of correlation analysis, the average grey values of the two analysed images are subtracted from the respective pixel value, so pixels contribute to the colocalisation coefficient in proportion to their intensity difference to the average rather than their absolute intensities. As a consequence, both ρ_p and ρ_c vary from -1 to 1 , i.e. perfect negative or positive correlation, perfect mutual exclusion, or perfect overlap of both fluorophores. However, the interpretation of the intermediate values is not straightforward. Therefore, Manders et al. (1993) proposed a slightly different formulation that takes the *overlap coefficient*

$$\rho_o = \frac{\sum_i^N w_1(i) \cdot w_2(i)}{\sqrt{\sum_i^N [w_1(i)]^2} \cdot \sqrt{\sum_i^N [w_2(i)]^2}} \quad (5.5)$$

as the starting point. ρ_o can assume values from 0 to 1 . Also, Eq. 5.5 is insensitive to differential photobleaching of both fluorophores, as is readily seen by substituting $w_j(i) = \alpha \cdot w'_j(i)$. However, ρ_o will create biased estimates for component images with very different intensities and very different densities of fluorescent particles. This effect can be cancelled out by splitting ρ_o into two different (but interdependent) coefficients,

$$\rho_o^2 = k_1 k_2, \quad (5.6a)$$

where

$$k_1 = \frac{\sum_i^N w_1(i) \cdot w_2(i)}{\sum_i^N [w_1(i)]^2} \quad (5.6b)$$

and

$$k_2 = \frac{\sum_i^N w_1(i) \cdot w_2(i)}{\sum_i^N [w_2(i)]^2}. \quad (5.6c)$$

The degree of colocalisation is expressed using two different parameters, the first measuring intensity differences relative to channel 1, the second relative to channel 2. Two new colocalisation coefficients can be defined from this which are proportional to the amount of fluorescence of the colocalising objects in each component image, relative to the total fluorescence in that component (Manders et al. 1993):

$$M_1 = \frac{\sum_i^N w'_1(i)}{\sum_i^N w_1(i)} \quad (5.7a)$$

and

$$M_2 = \frac{\sum_i^N w'_2(i)}{\sum_i^N w_2(i)}, \quad (5.7b)$$

where $w'_j(i) = w_j(i)$ if $w_{i \neq j}(i) > t$, and is zero otherwise. As before, t defines some intensity threshold. Alternatively, a spectral-angle map (Sect. 5.2.2.1) can be used as the basis for selecting a threshold. Thus, only pixels in the second component image that contribute some appreciable intensity (or display a certain degree of spectral resemblance with image $k \neq j$) contribute to the numerator of M_1 and do so in proportion to the total fluorescence in image 1. M_1 and M_2 can even be determined when the intensity differences between the component images are very large and can be thought of as a generalisation of Eq. 5.1, with the major difference that only their numerator is thresholded, but to the true intensity value, and is zero otherwise. Thus, instead of the overlapping pixel *area* alone, M_1 and M_2 weigh the area with the colocalised pixel *intensity*, i.e. they are – in some way – a hybrid between a pixel-based and an object-based measurement. The degree of colocalisation is defined as the ratio of the integral of the intensity distribution of colocalising pixels and the total intensity in the component image studied. When the number of pixels carrying an intensity above the threshold t is very different in images 1 and 2, M_1 and M_2 are a proper choice. Yet, the problems of thresholding, background subtraction, and treating outlier pixels remain, as with the other coefficients. A qualitative analysis of the factors that affect Manders's and Person's colocalisation coefficients is found in Garcia Peñarrubia et al. (2005).

Other methods for quantifying fluorophore colocalisation on a pixel-by-pixel basis have been described (Smallcombe 2001).

5.2.2.3 Regions of Interest and Segmenting Tools

Object-based colocalisation estimates, i.e. the segmentation of labels into distinct pixel clusters in three-dimensional space, followed by colocalisation of these clusters yield more reliable and sensitive measures of colocalisation than a simple determination of the number (or summed intensities) of colocalised pixels (pixel-based analysis). This is because object-based techniques utilise information about object shape and size in addition to intensity-information to sharpen the criteria used to designate colocalising pixels (Silver and Stryker 2000).

5.2.3 Object-Based Techniques

5.2.3.1 Threshold-Based Object Recognition

The simplest technique that does not rely on global intensity analysis was introduced by Lynch et al. (1991). Binary masks are created for both component

images by thresholding and the overlap between the thresholded *areas* is calculated (cf. Eq. 5.1). A similar approach is implemented in many imaging software packages. For example, the MetaMorph (Molecular Devices) COLOCAL drop-in allows the user to chose between different descriptors of overlap (area, average or integrated intensities in the region of overlap) in thresholded image (sub-) regions of interest. These parameter measurements can be transformed into a true quantitative colocalisation estimate using a trick (Becherer et al. 2003; Rappoport et al. 2003); by introducing an artificial pixel shift of one component image relative to the other and recalculating the parameters, one obtains a modified parameter. This is repeated, one pixel at a time, for, e.g. ten pixels in each direction and averaged over, e.g., the eight cardinal directions. The plot of the parameter measured with increasing deliberate misalignment of the two images allows the determination of a characteristic length scale on which both fluorophores colocalise. Irrespective of the choice of the intensity threshold made for each channel, the procedure is inherently *pixel-based*, i.e. within the regions of interest created the data are processed without introducing further assumptions for the object that is being imaged.

5.2.3.2 Localising Spots Using Segmented Image Subregions

Until now, we have treated images or even three-dimensional image stacks as large planar or cubic assemblies of independent pixels. One can – and indeed should – use the information contained in the image rather than treating each pixel individually. Although – mathematically speaking – the presence of image noise makes each pixel statistically independent of its neighbours, the intensity envelope, i.e. the low-spatial-frequency signal extending over an ensemble of nearby pixels, is not independent, owing to the diffraction limitation.

One example using correlated multipixel information is the accurate determination of the two-dimensional (or three-dimensional) *position* of point objects in a fluorescence image (or z-stack of images) (Ghosh and Webb 1994) by fitting a small region of the intensity image with a centre of mass (centroid) or two-dimensional Gaussian (Cheezum et al. 2001; Gennerich and Schild 2005) to locate the spot. Its position is calculated on the basis of all pixels that belong to the domain of the spot, so a meaningful contour must be delineated that defines the region on the image that belongs to the spot, e.g., using largest (Manders et al. 1996) or active (Dufour et al. 2005) contour spatial segmentation.

The object coordinate (rather than its intensity distribution) can then be used for the investigation of colocalisation. Spots are localised in *independent* image channels so that the accuracy of the particle position is not resolution-limited but rather depends on the signal-to-noise ratio of the fitted image and the measured PSF (Churchman et al. 2005; Karakikes et al. 2003; Morrison et al. 2003); therefore, the term *precision* rather than resolution is often used in this context. With bright molecular fluorophores, molecular distances can be measured with an accuracy better than 10 nm using conventional far-field optics (Lacoste et al. 2000; Michalet et al. 2001) and less than 2 nm using total internal reflection fluorescence

microscopy (Yildiz et al. 2003). Of course, for this precision to be attained the component images of the different colour channels must be truly independent, stressing the importance of eliminating cross-talk between images. Although this calculation is simple, its error analysis is demanding and has generally not been correctly applied (Churchman 2006).

When spectral overlap cannot be avoided, using the spatial distribution of fluorescence lifetimes instead of intensities can be an alternative (Berezovska et al. 2003; Brismar and Uifhake 1997; Heilemann et al. 2002; Wahl et al. 2004). In fluorescence lifetime imaging microscopy (FLIM), several (picosecond) time-resolved images of a sample are obtained at various time delays after pulsed laser excitation of the microscope field of view. Lifetimes are calculated pixel by pixel from these time-resolved images, and the spatial variations of the fluorescence lifetime are then displayed in a two-dimensional pseudocolour-coded map. Combining FLIM with polarisation-modulated excitation allows one to obtain, simultaneously, information about the relative orientation of fluorophores (Heinlein et al. 2005).

5.2.3.3 Studying Single-Pair Colocalisation and Interaction with Single-Molecule Fluorescence

Probably the most intuitive way of establishing colocalisation with object-based techniques is single-particle tracking. When two molecular fluorophores consistently move together, they are probably attached one to the other (Yang and Musser 2006). Dual-colour fluorescence cross-correlation spectroscopy (FCCS) is capable of measuring interacting fluorescently tagged macromolecules via temporal cross-correlation analysis of fluorescence intensity fluctuations collected from a small observation volume defined by the excitation beam focus (Schwille et al. 1997). Intensity fluctuations arising from changes in fluorophore concentration within the beam focus are recorded simultaneously in two channels and correlated in time to reveal transport properties and number densities of interacting and non-interacting species (reviewed in Bacia et al. 2006). Employing simultaneous two-photon excitation of three distinct dye species, Heinze et al. (2004) demonstrated their successful discrimination on a single-molecule level. This enables the direct observation of higher-order molecular complex formation in the confocal volume. Image cross-correlation spectroscopy (ICCS) relies on the same principles as FCCS, but utilises spatial correlation analysis of intensity fluctuations in fluorescence images (Brown et al. 1999). A quantitative comparison between the standard, fluorescence microscopy colocalisation algorithms and spatial ICCS has been published (Comeau et al. 2006). A similar double labelling and coincidence fluorescence detection method has been used to enhance the sensitivity of single-molecule detection and observe individual DNA molecules labelled with two different fluorophores in solution (Li et al. 2003). Single-molecule single-pair FRET (spFRET) experiments (Ha et al. 1996; Yang et al. 2006) extend these measurements to studying true molecular interaction (Allen et al. 2003; reviewed

in Yeh et al. 2005). Finally, bimolecular fluorescence complementation assays (Hu et al. 2002) in which two non-fluorescent protein fragments are combined to give a functional fluorophore may soon attain single-molecule sensitivity (reviewed in Hebert et al. 2006; Kerppola 2006; Piehler 2005).

All these techniques have in common that they rely on the ultrasensitive detection and identification, in extremis, of single molecular species. However, because of the faint signals involved, single-molecule techniques are particularly vulnerable to the incomplete separation of the different colour channels owing to the presence of autofluorescence, along with cross-excitation and emission bleed-through (see earlier). A SILU technique that uses the statistical correlations between pixels on the image single-diffraction-limited spots has been used to quantify the expression and colocalisation of about 15 copies of fluorescent protein molecules on single secretory vesicles (Nadrigny et al. 2006). Using classification and feature extraction techniques borrowed from multispectral and hyperspectral imaging techniques (see Box 5.3) and applied to microscopic imaging (reviewed in Zimmermann 2005), spectral unmixing improves FRET detection (Ecker et al. 2004; Gu et al. 2004; Neher and Neher 2004b).

5.3 Conclusions

- The resolving power of the instrument defines a three-dimensional minimal volume that gives the ‘unit cell’ for meaningful colocalisation analysis. For objects smaller than this volume, it is conceivable that both fluorophores are present in the same voxel accidentally without being associated.
- Colocalisation of intensity images is restricted to data sets with high signal-to-noise ratios and cannot provide colocalisation information at the low-intensity end.
- Image processing (filtering, deconvolution, unmixing) improves the colocalisation estimate, at the expense of spatial resolution. Appropriate controls must ascertain that artefacts that can be generated by image processing do not influence the estimate.
- Depending on the technique, the results of the colocalisation analysis differ qualitatively and quantitatively. Therefore, to allow data to be compared or reproduced, a detailed protocol must complement the colocalisation analysis.
- Irrespective of the precise technique used for estimating fluorophore presence and colocalisation, the reduction of a high-dimensional data set with millions of image elements to one or two numbers necessarily implies a considerable loss of information. Therefore, it is important to use a colocalisation measurement that extracts and preserves the information from the images that should be retained. Also, in analysing colocalisation, absolute numbers are often not terribly meaningful. Reporting relative parameter distributions and comparing the amount of colocalisation between different – spectrally equivalent – fluorescent markers can often be a sensible compromise.
- Single-molecule techniques are increasingly being used to localise and colocalise single fluorescently labelled biomolecules and, combined with FRET or fluores-

cence complementation analyses, to trace out molecular interactions. Owing to the faint intensities, these techniques are particularly vulnerable to spectral cross-talk and benefit from multispectral imaging and unmixing techniques.

While this chapter was in proof, Adler and Palmryd presented a normalised Pearson's coefficient for calculating co-localisation while taking into account image noise in the two detection channels. This approach based on comparing first the frame-to-frame variations within one color channel on replicate images and then calculating the corrected co-localisation estimate between the two channels. See I. Palmryd and J. Adler, *Making Accurate Measurement of Colocalization by Correcting for Image Noise*, 2007 Biophysical Society Meeting Abstracts, Biophysical Journal, Supplement, Abstract. p321a for details.

References

- Akner GM, K., Wilkström A, Sundqvist K, Gustafsson J (1991) Evidence for co-localisation of glucocorticoid receptor with cytoplasmic microtubules in human gingival fibroblasts, using two monoclonal anti-GR antibodies, confocal microscopy and image analysis. *J Steroid Biochem Mol Biol* 39:419–432
- Allen MW, Bieber Urbauer RJ, Zaidi A, Williams TD, Urbauer JL, Johnson CK (2003) Fluorescence labeling, purification, and immobilization of a double cysteine mutant calmodulin fusion protein for single-molecule experiments. *Anal Biochem* 325:273–284
- Axelrod D (2001) Selective imaging of surface fluorescence with very high aperture microscope objectives. *J Biomed Opt* 6:6–13
- Bacia K, Kim SA, Schwille P (2006) Fluorescence cross-correlation spectroscopy in living cells. *Nat Methods* 3:83–89
- Beaurepaire E, Mertz J (2002) Epifluorescence collection in two-photon microscopy. *Appl Opt* 41:5376–5382
- Becherer U, Moser T, Stuhmer W, Oheim M (2003) Calcium regulates exocytosis at the level of single vesicles. *Nat Neurosci* 6:846–853
- Berezovska O, Ramdy P, Skoch J, Wolfe MS, Bacsikai BJ, Hyman BT (2003) Amyloid precursor protein associates with a nicastrin-dependent docking site on the presenilin 1- γ -secretase complex in cells demonstrated by fluorescence lifetime imaging. *J Neurosci* 23:4560–4566
- Betz WJ, Mao F, Smith CB (1996) Imaging exocytosis and endocytosis. *Curr Opin Neurobiol* 6:365–371
- Betzig E, Patterson GH, Sougrat R, Lindwasser OW, Olenych S, Bonifacino JS, Davidson MW, Lippincott-Schwartz J, Hess HF (2006) Imaging intracellular fluorescent proteins at nanometer resolution. *Science* 313:1642–1645
- Blazer-Yost BL, Butterworth M, Hartman AD, Parker GE, Faletti CJ, Els WJ, Rhodes SJ (2001) Characterization and imaging of A6 epithelial cell clones expressing fluorescently labeled ENaC subunits. *Am J Physiol Cell Physiol* 281:C624–632
- Brismar H, Uifhake B (1997) Fluorescence lifetime measurements in confocal microscopy of neurons labeled with multiple fluorophores. *Nat Biotechnol* 15:373–377
- Brown CM, Roth MG, Henis YI, Petersen NO (1999) An internalization-competent influenza hemagglutinin mutant causes the redistribution of AP-2 to existing coated pits and is colocalized with AP-2 in clathrin free clusters. *Biochemistry* 38:15166–15173
- Brumback AC, Lieber JL, Angleson JK, Betz WJ (2004) Using FM1-43 to study neuropeptide granule dynamics and exocytosis. *Methods* 33:287–294
- Cheezum MK, Walker WF, Guilford WH (2001) Quantitative comparison of algorithms for tracking single fluorescent particles. *Biophys J* 81:2378–2388

- Chudakov DM, Chepurnykh TV, Belousov VV, Lukyanov S, Lukyanov KA (2006) Fast and precise protein tracking using repeated reversible photoactivation. *Traffic* 7:1304–1310
- Churchman LS, Okten Z, Rock RS, Dawson JF, Spudich JA (2005) Single molecule high-resolution colocalization of Cy3 and Cy5 attached to macromolecules measures intramolecular distances through time. *Proc Natl Acad Sci USA* 102:1419–1423
- Churchman LS, Flyvbjerg H, Spudich JA (2006) A non-Gaussian distribution quantifies distances measured with fluorescence localization techniques. *Biophys J* 90:668–671
- Comeau JWD, Costantino S, Wiseman PW (2006) A guide to accurate fluorescence microscopy colocalization measurements. *Biophys J* 91:4611–4622
- Cubitt AB, Heim R, Wollenweber LA (1999) Understanding structure-function relationships in the *Aequorea victoria* green fluorescent protein. In: Sullivan KF, Kay SA (eds) *Green fluorescent proteins*, vol. 58. Academic, San Diego, pp 19–33
- Demandolx D, Davoust J (1997) Multicolour analysis and local image correlation in confocal microscopy. *J Microsc* 185:21–36
- Dufour A, Shinin V, Tajbakhsh S, Guillen-Aghion N, Olivio-Marin JC, Zimmer C (2005) Segmenting and tracking fluorescent cells in dynamic 3-D microscopy with coupled active surfaces. *IEEE Trans Image Proc* 14:1396–1410
- Ecker RC, de Martin R, Steiner GE, Schmid JA (2004) Application of spectral imaging microscopy in cytomics and fluorescence resonance energy transfer (FRET) analysis. *Cytometry A* 59:172–181
- Finley KR, Davidson AE, Ekker SC (2001) Three-color imaging using fluorescent proteins in living zebrafish embryos. *BioTechniques* 31:66–70
- Friedman LJ, Chung J, Gelles J (2006) Viewing dynamic assembly of molecular complexes by multi-wavelength single-molecule fluorescence. *Biophys J* 91:1023–1031
- Garcia Peñarrubia P, Férez Ruiz X, Galvez J (2005) Quantitative analysis of the factors that affect the determination of colocalization coefficients in dual-color confocal images. *IEEE Trans Image Proc* 14:1–8
- Gennerich A, Schild D (2005) Sizing-up finite fluorescent particles with nanometer-scale precision by convolution and correlation image analysis. *Eur Biophys J* 34:181–199
- Ghosh RN, Webb WW (1994) Automated detection and tracking of individual and clustered cell surface low density lipoprotein receptor molecules. *Biophys J* 66:1301–1318
- Giepmans BNG, Adams SR, Ellisman MH, Tsien RY (2006) The fluorescent toolbox for assessing protein location and function. *Science* 312:217–224
- Gonzales RC, Wintz P (1987) Digital image processing. Addison-Wesley, Reading
- Griesbeck O (2004) Fluorescent proteins as sensors for cellular functions. *Curr Opin Neurobiol* 14:636–641
- Gu Y, Di WL, Kelsell DP, Zicha D (2004) Quantitative fluorescence resonance energy transfer (FRET) measurement with acceptor photobleaching and spectral unmixing. *J Microsc* 215:162–173
- Gustafsson MGL (2005) Nonlinear structured-illumination microscopy: wide-field fluorescence imaging with theoretically unlimited resolution. *Proc Natl Acad Sci USA* 102:13081–13086
- Ha T, Enderle T, Ogletree DF, Chemla DS, Selvin PR, Weiss S (1996) Probing the interaction between two single molecules: fluorescence resonance energy transfer between a single donor and a single acceptor. *Proc Natl Acad Sci USA* 93:6264–6268
- Hebert TE, Gales C, Rebois RV (2006) Detecting and imaging protein-protein interactions during g protein-mediated signal transduction *in vivo* and *in situ* by using fluorescence-based techniques. *Cell Biochem Biophys* 45:85–109
- Heilemann M, Herten D-P, Heintzmann R, Cremer C, Müller C, Tinnefeld P, Weston KD, Wolfrum J, Sauer M (2002) High-resolution colocalization of single dye molecules by fluorescence lifetime imaging microscopy. *Anal Chem* 74:3511–3517
- Heinlein T, Biebricher P, Schlüter C, Roth M, Herten D-P, Wolfrum J, Heilemann M, Müller C, Tinnefeld P, Sauer M (2005) High-resolution colocalization of single molecules within the resolution gap of far-field microscopy. *ChemPhysChem* 6:949–955

- Heinze K, Jahnz M, Schwille P (2004) Triple-color coincidence analysis: One step further in following higher order molecular complex formation. *Biophys J* 86:506–516
- Henkel AW, Lübbe J, Betz WJ (1996) Fm1-43 dye ultrastructural localization in and release from frog motor nerve terminals. *Proc Natl Acad Sci USA* 93:1918–1923
- Hess ST, Girirajan TP, Mason MD (2006) Ultra-high resolution imaging by fluorescence photoactivation localization microscopy (FPALM). *Biophys J* 91:4258–4272
- Hirrlinger PG, Scheller A, Braun C, Quintela-Schneider M, Fuss B, Hirrlinger J, Kirchhoff F (2005) Expression of red coral fluorescent proteins in the central nervous system of transgenic mice. *Mol Cell Neurosci* 30:291–303
- Hofmann M, Eggeling C, Jakobs S, Hell SW (2005) Breaking the diffraction barrier in fluorescence microscopy at low light intensities by using reversibly photoswitchable proteins. *Proc Natl Acad Sci USA* 102:17565–17569
- Hu C-D, Chinenov Y, Kerppola TK (2002) Visualization of interactions among bZIP and Rel family proteins in living cells using bimolecular fluorescence complementation. *Mol Cell* 9:789–798
- Jares-Erijman EA, Jovin TM (2003) FRET imaging. *Nat Biotechnol* 21:1387–1395
- Jomphe C, Bourque M-J, Fortin GD, St-Gelais F, Okano H, Kobayashi K, Trudeau L-E (2005) Use of TH-EGFP transgenic mice as a source of identified dopaminergic neurons for physiological studies in postnatal cell culture. *J Neurosci Methods* 146:1–12
- Karakikes I, Barber RE, Morrison IEG, Fernandez N, Cherry RJ (2003) Co-localization of cell surface receptors at high spatial resolution by single-particle fluorescence imaging. *Biochem Soc Trans* 31:1453–1455
- Kerppola TK (2006) Visualization of molecular interactions by fluorescence complementation. *Nat Rev Mol Cell Biol* 7:449–456
- Kozubek M, Matula P (2000) An efficient algorithm for measurement and correction of chromatic aberrations in fluorescence microscopy. *J Microsc* 200:206–217
- Kruse FA, Lefkoff AB, Boardman JW, Heidereth KB, Shapiro AT, Barloon JP, Goetz AF (1993) The spectral image processing system (SIPS) – interactive visualization and analysis of imaging spectrometer data. *Remote Sens Environ* 44:145–163
- Lacoste TD, Michalet X, Pinaud F, Chemla DS, Alivisatos AP, Weiss S (2000) Ultrahigh-resolution multicolor colocalization of single fluorescent probes. *Proc Natl Acad Sci USA* 97:9461–9466
- Landmann L (2002) Deconvolution improves colocalization analysis of multiple fluorochromes in 3D confocal data sets more than filtering techniques. *J Microsc* 208:134–147
- Li D, Xiong J, Qu A, Xu T (2004) Three-dimensional tracking of single secretory granules in live PC12 cells. *Biophys J* 87:1991–2001
- Li H, Ying L, Green JJ, Basasubramanian S, Klenerman D (2003) Ultrasensitive coincidence fluorescence detection of single DNA molecules. *Anal Chem* 75:1664–1670
- Lowy RJ (1995) Evaluation of triple-band filters for quantitative epifluorescence microscopy. *J Microsc* 178:240–250
- Lynch RM, Fogarty KE, Fay FS (1991) Modulation of hexokinase association with mitochondria analyzed with quantitative three-dimensional confocal microscopy. *J Cell Biol* 112:385–395
- Manders EM, Stap J, Brakenhoff GJ, van Driel R, Aten JA (1992) Dynamics of three-dimensional replication patterns during the S-phase, analysed by double labelling of DNA and confocal microscopy. *J Cell Sci* 103:857–862
- Manders EM, Verbeek FJ, Aten JA (1993) Measurement of co-localization of objects in dual-colour confocal images. *J Microsc* 169:375–382
- Manders EM, Hoebe R, Strackee J, Vossepoel AM, Aten JA (1996) Largest-contour segmentation: a tool for the localization of spots in confocal images. *Cytometry* 23:15–21
- Martinez-Arcas S, Rudge R, Vacca M, Raposo G, Camonis J, Proux-Gillardeaux V, Daviet L, Formstecher E, Hamburger A, Filippini F, D'Esposito M, Galli T (2003) A dual mechanism controlling the localization and function of exocytic v-SNAREs. *Proc Natl Acad Sci USA* 100:9011–9016

- Messler P, Harz H, Uhl R (1996) Instrumentation for multiwavelengths excitation imaging. *J Neurosci Methods* 69:137–147
- Michalet X, Lacoste TD, Weiss S (2001) Ultrahigh-resolution colocalization of spectrally separable point-like fluorescent probes. *Methods* 25:87–102
- Miyashita T (2004) Confocal microscopy for intracellular co-localization of proteins. In: Fu H (ed) Protein-protein interactions methods and applications, vol 261. Humana, Totowa, pp 399–410
- Miyawaki A (2005) Innovations in the imaging of brain functions using fluorescent proteins. *Neuron* 48:189–199
- Morrison IEG, Karakikes I, Barber RE, Fernandez N, Cherry RJ (2003) Detecting and quantifying colocalization of cell surface molecules by single particle fluorescence imaging. *Biophys J* 85:4110–4121
- Nadrigny F, Rivals I, Hirrlinger PG, Koulakoff A, Personnaz L, Vernet M, Allioux M, Chaumeil M, Ropert N, Giaume C, Kirchhoff F, Oheim M (2006) Detecting fluorescent protein expression and colocalisation on single secretory vesicles with linear spectral unmixing. *Eur Biophys J* 35:533–547
- Nadrigny F, Li D, Kemnitz K, Ropert N, Koulakoff A, Rudolph S, Vitali M, Giaume C, Kirchhoff F, Oheim M. Systematic Co-localization Errors between Acridine Orange and EGFP in Astrocyte Vesicular Organelles. *Biophys J.* 2007 Apr 6; [Epub ahead of print]
- Neher R, Neher E (2004a) Optimizing imaging parameters for the separation of multiple labels in a fluorescence image. *J Microsc* 213:46–62
- Neher RA, Neher E (2004b) Applying spectral fingerprinting to the analysis of fret images. *Microsc Res Tech* 64:185–195
- Neteler M, Grasso D, Michelazzi I, Miori L, Merler S, Furlanello C (2004) New image processing tools for grass. In: Proceedings of FOSS/GRASS user conference 2004, Bangkok, Thailand
- Oheim M, Loerke D, Stühmer W, Chow RH (1999) Multiple stimulation-dependent processes regulate the size of the releasable pool of vesicles. *Eur Biophys J* 28:91–101
- Oheim M, Beaurepaire E, Chaigneau E, Mertz J, Charpak S (2001) Two-photon microscopy in brain tissue: Parameters influencing the imaging depth. *J Neurosci Methods* 111:29–37
- Oheim M, Li D, Luccardini C, Yakovlev A (2007) Online resource for calculating the spectral separability index Xijk. <http://www.biomedicale.univ-paris5.fr/neurophysiologie/Groups/oheimpropertgroup.php>. Cited 4 Apr 2007
- Oshiro M, Moomaw B (2003) Cooled vs. intensified vs. electron bombardment CCD cameras – applications and relative advantages. *Methods Cell Biol* 72:133–156
- Patterson GH, Knobel SM, Sharif WD, Kain SR, Piston DW (1997) Use of the green fluorescent protein and its mutants in quantitative fluorescence microscopy. *Biophys J* 73:2782–2790
- Piehler J (2005) New methodologies for measuring protein interactions in vivo and in vitro. *Curr Opin Struct Biol* 15:4–14
- Rapoport JZ, Taha BW, Lemeer S, Benmerah A, Simon SM (2003) The AP-2 complex is excluded from the dynamic population of plasma membrane-associated clathrin. *J Biol Chem* 278:47357–47360
- Rodgers W (2002) An automated method for quantifying fluorophore colocalization in fluorescence double-labeling experiments. *BioTechniques* 32:28–34
- Schultz C, Schleifenbaum A, Goedhart J, Gadella TW Jr (2005) Multiparameter imaging for the analysis of intracellular signaling. *Chembiochem* 8:1323–1330
- Schwille P, Meyer-Almes FJ, Rigler R (1997) Dual-color fluorescence cross-correlation spectroscopy for multicomponent diffusional analysis in solution. *Biophys J* 72:1878–1886
- Shaner N, Steinbach PA, Tsien RY (2005) A guide to choosing fluorescent proteins. *Nat Methods* 2:905–909
- Sharp MD, Poglano K (1999) An in vivo membrane fusion assay implicates spoIIIE in the final stages of engulfment during *Bacillus subtilis* sporulation. *Proc Natl Acad Sci USA* 96:14553–14558
- Sheppard CJR, Gan X, Gu M, Roy M (1995) Signal-to-noise in confocal microscopes. In: Pawley JB (ed) Handbook of confocal microscopy Plenum, New York

- Shoji J-Y, Arioka M, Kitamoto K (2006) Vacuolar membrane dynamics in the filamentous fungus *Aspergillus oryzae*. *Eukaryot Cell* 5:411–421
- Shrestha DP, Margate DE, van der Meer F, Anh HV (2005) Analysis and classification of hyperspectral data for mapping land degradation: an application in southern Spain. *Int J Appl Earth Obs Geoinf* 7:85–96
- Silver MA, Stryker MP (2000) A method for measuring colocalization of presynaptic markers with anatomically labelled axons using double label immunofluorescence and confocal microscopy. *J Neurosci Methods* 94:205–215
- Smallcombe A (2001) Multicolor imaging: the important question of co-localization. *BioTechniques* 30:1240–1246
- Stauffer TP, Meyer T (1997) Compartmentalized IgE receptor-mediated signal transduction in living cells. *J Cell Biol* 139:1447–1457
- Theer P, Hasan MT, Denk W (2003) Two-photon imaging to a depth of 1000 microns in living brains by use of a Ti:Al₂O₃ regenerative amplifier. *Opt Lett* 28:1022–1024
- Tyler WJ, Zhang X-L, Hartman K, Winterer J, Muller W, Stanton PK, Pozzo-Miller L (2006) Bdnf increases release probability and the size of a rapidly recycling vesicle pool within rat hippocampal excitatory synapses. *J Physiol* 574:787–803
- Wahl M, Koberling F, Patting M, Rahn H, Erdmann R (2004) Time-resolved confocal fluorescence imaging and spectroscopy system with single molecule sensitivity and sub-micrometer resolution. *Curr Pharm Biotechnol* 5:299–308
- Wessendorf MW, Brelje TC (1992) Which fluorophore is brightest? A comparison off the staining obtained using fluorescein, tetramethylrhodamine, lissamine rhodamine, Texas Red, and cyanine 3.18. *Histochemistry* 98:81–85
- Willig KI, Kellner RR, Medda R, Hein B, Jakobs S, Hell SW (2006) Nanoscale resolution in GFP-based microscopy. *Nat Methods* 3:721–723
- Xia J, Kim SHH, Macmillan S, Truant R (2006) Practical three color live cell imaging by wide-field microscopy. *Biol Proc Online* 8:63–68
- Yang J, Chen H, Vlahov IR, Cheng J-X, Low PS (2006) Evaluation of disulfide reduction during receptor-mediated endocytosis by using FRET imaging. *Proc Natl Acad Sci USA* 103:13872–13877
- Yang W, Musser SM (2006) Visualizing single molecules interacting with nuclear pore complexes by narrow-field epifluorescence microscopy. *Methods* 39:316–328
- Yeh HC, Chao SY, Ho YP, Wang TH (2005) Single-molecule detection and probe strategies for rapid and ultrasensitive genomic detection. *Curr Pharm Biotechnol* 6:453–461
- Yildiz A, Forkey JN, McKinney SA, Ha T, Goldman YE, Selvin PR (2003) Myosin v walks hand-over-hand: Single fluorophore imaging with 1.5-nm localization. *Science* 300:2061–2065
- Zimmermann T (2005) Spectral imaging and linear unmixing in light microscopy. *Adv Biochem Eng Biotechnol* 95:245–265